Sole marks reveal deep-marine depositional process and environment: implications for flow transformation and hybrid-event-bed models

JACO H. BAAS,[1] NIALL D. TRACEY,[1*] and JEFF PEAKALL[2]

[1] School of Ocean Sciences, Bangor University, Menai Bridge, Anglesey LL59 5AB, U.K.

[2] School of Earth & Environment, University of Leeds, L2 9JT, U.K.

** Now at Department of Earth Sciences, Durham University, DH1 3LE, U.K.*

e-mail: j.baas@bangor.ac.uk

ABSTRACT

Deposits of sediment gravity flows in the Aberystwyth Grits Group (Silurian, west Wales, United Kingdom) display evidence that sole marks are suitable for reconstructing depositional processes and environments in deep-marine sedimentary successions. Based on drone imagery, 3D laser scanning, high-resolution sedimentary logging, and detailed descriptions of sole marks, an outcrop 1600 m long between the villages of Aberarth and Llannon was subdivided into seven lithological units, representing: (a) mudstone-poor, coarse-grained and thick-bedded submarine channel fills, dominated by the deposits of erosive high-density turbidity currents with flute marks; (b) mudstone-rich levee deposits with thin-bedded, fine-grained sandstones formed by low-density turbidity currents that scoured the bed to form flute marks; (c) channel–lobe transition-zone deposits, dominated by thick beds, formed by weakly erosive, coarse-grained hybrid events, with pronounced mudstone-rich or sandstone-dominated debritic divisions and groove marks below basal turbiditic divisions, and with subordinate amounts of turbidites and debris-flow deposits; (d) tabular, medium- to thick-bedded turbiditic sandstones with flute marks and mixed sandstone–mudstone hybrid event beds mainly with groove marks, interpreted as submarine lobe-axis (or off-axis) deposits; and (e) tabular, thin- to medium-bedded, fine-grained, mainly turbiditic sandstones mostly with flute marks, formed in a lobe-fringe environment. Both lobe environments also comprised turbidites with low-amplitude bed waves and large ripples, which are interpreted to represent transient-turbulent flows. The strong relationship between flute marks and turbidites agrees with earlier predictions that turbulent shear flows are essential for the formation of flute marks. Moreover, the observation as part of this study that debris-flow deposits are exclusively associated with groove marks signifies that clay-charged, laminar flows are carriers for tools that are in continuous contact with the bed. A new process model for hybrid event beds, informed by the dominance of tool marks, in particular grooves, below the basal sand division (H1 division of Haughton et al. 2009, Marine and Petroleum Geology, v. 26, p. 1900–1918) and by the rapid change from turbidites in the channel to hybrid event beds in the channel–lobe transition zone, is proposed. This model incorporates profound erosion of clay in the channel by the head of a high-density turbidity current and subsequent transformation of the head into a debris flow following rapid lateral flow expansion at the mouth of the channel. This debris flow forms the groove marks below the H1 division in hybrid event beds. A temporal increase in cohesivity in the body of the hybrid event is used to explain the generation of the H1, H2, and H3 divisions (*sensu* Haughton et al. 2009) on top of the groove surfaces, involving a combination of longitudinal segregation of bedload and vertical segregation of suspension load. This study thus demonstrates that sole marks can be an integral part of sedimentological studies at different scales, well beyond their traditional use as indicators of paleoflow direction or orientation.

INTRODUCTION

Sole Marks: the Basics

The bases of sediment-gravity-flow (SGF) deposits in deep-marine sedimentary successions commonly contain sole structures (e.g., Dżułyński and Walton 1965; Peakall et al. 2020). These sole structures, which are the product of erosion of the underlying sediment surface, can be classified into two types:

scour marks and tool marks (Dżułyński and Sanders 1962; Collinson and Mountney 2019). Since their discovery by Hall (1843), sole marks have been used routinely as paleoflow direction and orientation indicators. Pioneering laboratory experiments and fieldwork on type, form, and origin of sole marks were done mainly in the 1960s and 1970s (e.g., Dżułyński 1965; Allen 1971). However, it has recently been advocated that sole-mark type could also be associated with flow type and, by inference, with deposit type, particularly for depositional, non-bypassing flow (Peakall et al. 2020). The model of Peakall et al. (2020), summarized in Fig. 1, also proposes that, as different morphological elements in submarine depositional systems can exhibit unique sets of flow and deposit types, sole marks may also store information on type of morphological element and distance along submarine depositional systems (cf. Dirnerová and Janočko 2014). The present paper provides field data from the deep-marine Aberystwyth Grits Group (Silurian, West Wales, U.K.) that, for the first time, critically assess the relationships between sole-mark type and flow properties, deposit type, and type of depositional environment that underpin the model of Peakall et al. (2020), and use these relationships to aid process models for SGFs.

Sole-Mark Types

The *flute mark* is the most common type of scour mark (Fig. 2A) (Enos 1969; Reineck and Singh 1973; Allen 1984). In the natural environment, the *parabolic flute mark* is most common (Fig. 2A); this form is closely described by the ideal flute mark of Allen (1971, 1984). Other subclasses of flute mark are spindle flutes and asymmetric flutes. *Spindle flutes* are shallower and more elongated than parabolic flutes (Allen 1971, 1984). *Asymmetrical flutes* have furrows and ridges that decrease in size in an outward direction on one side, with occasionally a corkscrewed or twisted head (Allen 1984).

Tool marks comprise continuous and discontinuous varieties (e.g., Dżułyński and Radomski 1955). Continuous tool marks are produced by a tool continually interacting with the bed, thus creating a mark that is typically longer than the size of the outcrop (Dżułyński and Walton 1965). Continuous tool marks include *groove marks* (Fig. 2B) (Enos 1969; Middleton and Hampton 1973, 1976) and *chevron* *marks* (Fig. 2C) (Allen, 1984). Groove marks consist of an elongated ridge of constant depth and width that runs along the base of an SGF deposit, inferred to form as a tool is dragged along a soft bed in a laminar flow (Draganits et al. 2008) and more specifically by a flow with sufficient cohesive strength to hold a clast in a fixed position (Peakall et al. 2020). Chevron marks are created by fluid stressing of weakly consolidated muds via the shedding of eddies from the wakes of tools that move close to the bed (Allen 1984). Chevrons are preserved as V-shaped or U-shaped ridges that point in a downstream direction (Craig and Walton 1962; Allen 1984).

Discontinuous tool marks (Fig. 3) are formed by objects interacting intermittently with a soft substrate, thereby generating an impact feature (Allen 1984). Discontinuous tool marks can be further subdivided into prod marks, skip marks, tumble marks, and skim marks (Dżułyński and Sanders 1962; Allen 1984). A *prod mark* forms when an elongated tool impacts the bed in a downward-dipping manner and then abruptly exits the bed (Allen 1984) (Fig. 3), thus producing transversely asymmetrical marks with a gentle, longitudinal stoss side and a steep lee side (Dżułyński et al. 1959; Allen 1984). A *skip mark* is formed by a tool creating a series of evenly spaced, similarly shaped, imprints, spaced not much more than the length of the tool (Allen 1984) (Fig. 3). *Tumble marks* (Fig. 2D) are a specific type of skip mark, formed by an angular tool that repeatedly imprints an edge as the tool somersaults along the bed (Fig. 3) (Peakall et al. 2020). Objects that skim along a bed in a gently curving concave-up trajectory can plough sediment out of the way generating a *skim mark* (Dżułyński et al. 1959; Allen 1984) (Fig. 3). Skim marks are generally longer than they are wide and longitudinally symmetrical (Fig. 3).

Relationship of Sole Marks to Flow Type

Depending mainly on flow velocity, sediment type, and clay concentration, SGFs can exhibit different flow behaviors in between turbulent and laminar end members (Fig. 4; Wang and Plate 1996; Baas et al. 2016a; Baker et al. 2017; Hermidas et al. 2018). Peakall et al. (2020) associated these flow behaviors with specific types of sole mark. Turbulent flows (Fig. 4A), which include most turbidity currents, have been suggested to produce predominantly flute marks (Allen 1968, 1971), in particular parabolic flute marks (Fig. 1; Peakall et al. 2020). The high turbulence intensities in turbulence-enhanced transitional flow (Fig. 4B) allow for more substantial erosion (Baas et al. 2009, 2011), which has been suggested to generate flutes that are bulbous and larger than in turbulent flow (Fig. 1; Peakall et al. 2020). Turbulence-enhanced transitional flow evolves into lower transitional plug flow (Fig. 4C), as the clay concentration is increased (Baas et al. 2009, 2011, 2016b). Damping of turbulence in the plug of lower transitional plug flows has been associated with the production of smaller parabolic flutes than in turbulent flow and turbulence-enhanced transitional flow (Fig. 1; Peakall et al. 2020). Progressive turbulence damping upon a change from lower to upper transitional plug flow (Fig. 4D; Baas et al. 2009, 2011, 2016b) has been suggested to further decrease flute size, and lead to the formation of spindle flutes, eventually stopping the generation of flutes altogether (Peakall et al. 2020). Instead, prod marks followed by skim marks are predicted to form, governed by buoyancy forces that are high enough to keep tools in suspension intermittently (Fig. 1; Peakall et al. 2020). Upper transitional plug flow evolves into quasi-laminar plug flow and then laminar plug flow if clay concentration is increased in such a way that the base of the rigid plug approaches the bed. These flows are equivalent to mud flows and debris flows in deep-marine environments (Baas et al. 2011). At the lower end of quasi-laminar plug flow, skip marks have been proposed to be the dominant type of tool mark (Peakall et al. 2020). These skip marks are replaced by chevron marks and groove marks in upper quasi-laminar plug flow and laminar plug flow, where the tools can neither move vertically nor rotate (Peakall et al. 2020).

Sole Marks and Hybrid Event Beds

Mixed sand–mud hybrid event beds (e.g., Haughton et al. 2009; Kane and Pontén 2012) are a prime example of a type of deposit that has been linked to specific morphological elements, primarily the fringes of submarine lobes (e.g., Haughton et al. 2003; Hodgson 2009; Grundvåg et al. 2014; Spychala et al. 2017a, 2017b). Hybrid event beds are also present in basin-floor sheet systems beyond lobes and in some proximal locations, including channel–lobe transition zones and proximal lobes, reflecting rapid flow transformation (in several cases over 100s of meters) after large-scale erosion of mud (e.g., Fonnesu et al. 2015, 2018; Brooks et al. 2018; Mueller et al. 2021). Moreover, Terlaky and Arnott (2014) described hybrid event beds in avulsion lobes. Ideal hybrid event beds consist of five vertically stacked divisions (Haughton et al. 2009; Baas et al. 2011): (H1) basal massive sand formed by deposition from a high-density turbidity current or a transient-turbulent flow without sufficient turbulence and cohesive support; (H2) banded heterolithic sand–mud formed by a transitional flow with intermittent or modulated turbulence; (H3) chaotically mixed sand–mud, with or without mud clasts, associated with a cohesive debris flow; (H4) laminated sand generated by a low-density turbidity current; and (H5) structureless mud formed by suspension fallout from the tail of a low-density turbidity current. Although present in a variety of locations, sole marks formed by these turbulence-modulated hybrid flows may be less common in locations that are more proximal than lobe fringes, such as submarine channels where flows typically are more turbulent (Peakall and Sumner 2015), although they can be present in channel–lobe transition zones and proximal lobes in cases where large-scale erosion of mud takes place.

Research Aims

The model of Peakall et al. (2020) for the relationship between sole marks and paleohydraulics (Fig. 1) was informed by a combination of literature-based experimental data and field observations, theoretical considerations, and novel hypotheses. This model built upon ground-breaking, but now largely dormant, research in the 1960s and 1970s by, for example, Dżułyński (1965) and Allen (1971). However, this pioneering research has since been almost exclusively used to reconstruct paleoflow directions and orientations. In order to fully benefit the geological community, Fig. 1, as well as further inferences made by Peakall et al. (2020), need verification in natural environments, using recent advances in our understanding of the deposits of laminar, transitional, and turbulent flows in core and outcrop (e.g., Kane and Pontén 2012; Fonnesu et al. 2015; Baker and Baas 2020). The main aim of the present paper was to test key aspects of Peakall et al.'s (2020) model in the deep-marine Aberystwyth

Grits Group (Silurian, West Wales, United Kingdom), where a variety of well-preserved sole marks below SGF deposits highly polished by wave action are exposed in coastal outcrops. The following specific research questions were investigated:

1. Does a predictable relationship between sole-mark type and size and depositional process exist in the Aberystwyth Grits Group?
2. Is there a link between sole-mark type and size and their inferred position in the depositional system that formed the Aberystwyth Grits Group?
3. Do these relationships agree with the predictions of Peakall et al. (2020) and thus provide a generic aid in reconstructing the processes that generate deep-marine sedimentary architecture?

GEOLOGICAL SETTING

The Aberystwyth Grits Group forms part of the deep-marine sedimentary fill of the Welsh Basin in the Llandovery epoch of the Silurian (Fig. 5). At this time, c. 435 million years ago, the Welsh Basin experienced extensional faulting related to the oblique closure of the Iapetus Ocean during the collision between the microcontinent of Avalonia in the South and Laurentia in the North (Schofield et al. 2008). This extensional faulting was accompanied by uplift of the hinterland, which became a southwestern source of sediment for the Welsh Basin. At the same time, major subsidence created accommodation space in the Welsh Basin that was filled with thick successions of SGF deposits (Cherns et al. 2006), including the Aberystwyth Grits Group (Baker and Baas 2020). Previous studies have proposed that the Aberystwyth Grits Group formed in a linear fault-controlled trough that was confined to the east and southeast by the Bronnant Fault (Wilson et al. 1992; Smith 2004; Cherns et al. 2006; Gladstone et al. 2018). McClelland et al. (2011) established a decrease in average grain size and bed thickness both northeastward down the sub-basin and stratigraphically upward. In the study area between Aberarth and Llannon (Fig. 6), the Aberystwyth Grits Group consists of a typical deep-marine succession of SGF facies alternating with muddy hemipelagic facies (e.g., Wood and Smith

1958). The SGF facies are composed of siltstone and sandstone, with occasional granule-rich deposits, and event-bed thickness ranges from several tens of millimeters to c. 1.5 m. Wood and Smith (1958) distinguished turbidity current deposits and mixed sandstones–mudstones with distinct internal soft-sediment deformation that have since been interpreted as hybrid event beds (Talling et al. 2004). Cherns et al. (2006) proposed that the lithofacies between Aberarth and Llannon were deposited in the off-axis regions of submarine lobes.

METHODS

Field Data

Sedimentological data were collected from coastal outcrops in the Aberystwyth Grits Group between Aberarth and Llannon (Fig. 6), using drone imagery, 3D laser scanning, high-resolution sedimentary logging, and detailed descriptions of sole marks. This integration of methods allowed the 1,600-m-long outcrop to be subdivided into seven units, based on changes in lithology. The general properties and stacking patterns of sedimentary facies in these units were captured in graphic logs, between 5 and 10 m thick. Thereafter, detailed logs of representative event beds with sole marks were collected in each unit, totaling 32 beds. Standard logging of textural, structural, and morphological properties was accompanied by the determination of types, dimensions, and orientation of sole marks (Zervas et al. 2009). Crosscutting relationships between sole marks were considered as evidence for bypassing of the flows that formed the older sole marks (Peakall et al. 2020). The presence of sole marks with paleoflow directions that differed by more than 10° were also taken into account as evidence for bypassing. These criteria for bypass were not used for grooves because these sole marks regularly crosscut and have different paleoflow directions on lower bed surfaces formed by a single flow (Peakall et al. 2020). In addition to the high-resolution logs, a further 38 beds with sole marks were described more generally in terms of deposit type and thickness, sole structure type and size, and evidence for bypass.

A DJI Inspire two drone (quadcopter) equipped with a gimbal-mounted high-resolution camera was used to conduct an aerial survey along most of the length and height of the outcrop (Fig. 6). The drone captured digital photographs of the outcrop at a down-facing angle of 30^{o} and at three different altitudes: 12 m, 20 m, and 80 m above the base of the cliff face. The drone was flown manually along the cliff face at each altitude. The photographs overlapped by at least 10%, thus ensuring a continuous record of the architecture of the AGG at this location.

Two sites were selected for 3D scanning, using a Leica Geosystems ScanStation C10 (Fig. 6) attached to a tripod. Site 1 was rich in sandstone and covered inferred channel-fill, levee, and channel–lobe transition-zone successions. Site 2 covered a range of well-defined sole-mark types, including rare chevron marks. At Site 1, four medium-resolution (50 mm) and three high-resolution laser scans (1 mm) (Schmitz et al. 2019) were conducted. At Site 2, three medium-resolution scans and one high-resolution laser scan were collected. This procedure assured maximum possible coverage of the outcrop at both sites. The laser scanner followed a predetermined 360^{o} coverage route and, after each scan, the scanner repeated the same route taking true-color photographs. Both sites were geo-referenced using target discs and spheres and an RTK GPS device (Leica GNSS GS18 with CS20 handset) (Humair et al. 2015).

Data Processing

In each unit, the sedimentological data were used to retrieve relationships between depositional environment, turbulent, transitional, and laminar flow types, and sole-mark type and size, accounting for evidence of bypassing flows.

The Hugin software was used to automatically stitch together the drone photographs. Thereafter, unit boundaries and selected event beds in these units were traced, across faults where appropriate, to aid the reconstruction of the sedimentary architecture of the Aberystywth Grits Group at the study site.

The Leica Cyclone software package was used to produce a 3D point cloud model of the outcrops at Sites 1 and 2, making sure to snip out scanned data that were not part of these outcrops. The true-color photographs were then draped onto the 3D point cloud model to create a 3D color image of the outcrops at both sites. These data were then exported as an xyz file to the Truview V2 software to measure the dimensions of sediment beds and sole marks. These data complemented dimensional data obtained with a tape measure at easily accessible locations.

RECONSTRUCTION OF DEPOSITIONAL PROCESSES AND ENVIRONMENT

Description of Lithological Units

The coastal outcrop studied between Aberarth and Llannon was subdivided into seven vertically stacked lithological units, based on general architectural expression, sandstone-to-mudstone ratio, event bed thickness, degree of sandstone bed amalgamation, and sedimentary facies. Figures 7 to 9 show original and interpreted composite images of the southern, middle, and northern part of the outcrop covered by the drone and the 3D scanner, which contain lithological Units 2 to 6. Units 1 and 7 are to the south and north of the cliff section shown in Figures 7 and 9, respectively.

Units 1, 3, and 7.—Units 1, 3, and 7 consist of tabular, predominantly thick-bedded sandstones and mixed sandstones–mudstones interbedded with thin-bedded to medium-bedded mudstones (Figures 7, 10). The cumulative thickness of the mudstone beds is 20% of the total thickness in all three units. The sandstones are fine-grained to medium-grained, with coarse-grained to very coarse-grained basal divisions. Two beds in the logged part of Unit 7 are rich in granule-size clasts (Fig. 10C). Erosional contacts, tens of millimeters deep, between some sandstones and the underlying mudstones as well as occasional sandstone bed amalgamation (e.g., between 4.05 m and 4.7 m in Fig. 10A and in the lower log in Fig. 10C) distinguish these units from the units with lower cumulative mudstone bed thickness and thinner-bedded sandstones. Many beds exhibit convolute and contorted bedding (e.g., 5.45–6 m in Fig. 10A), chaotic mixtures of sandstone and mudstone (e.g., 4.05–5.3 m in Fig. 10A), mudstone rafts and clasts (e.g., at 0.4 m in Fig. 10A), sandstone clasts (e.g., in Beds 7b and 7d in Fig. 10C), vertical fluid-escape structures (e.g., Bed 7b in Fig. 10C), load casts, and foundered sand (e.g., 0.45–0.9 m in Fig. 10B). These structures usually occur in muddy sandstones or sandy mudstones juxtaposed with relatively clean sandstones, which are often massive and structureless, and they may contain mudstone clasts (e.g., in the lower half of the log shown in Fig. 10A). Plane-parallel lamination and ripple cross-lamination are uncommon in Units 1, 3, and 7, and mostly confined to thin-bedded, fine- to very-fine grained sandstones and thin divisions in thicker sandstones (e.g., Fig. 10A).

Unit 2.—Unit 2 comprises a vertical succession of tabular, mostly thin-bedded and very-fine grained or fine-grained sandstones interbedded with thin-bedded to medium-bedded mudstones (Fig. 7). The cumulative mudstone bed thickness is 55% of the total thickness. The sandstones are mud-poor, vertically graded, and rich in plane-parallel lamination and ripple cross-lamination organized in incomplete Bouma sequences (Bouma 1962) (Fig. 11A). Some relatively thick sandstone beds have a lower massive, structureless division, and ripple cross-lamination is regularly modified to convolute bedding. Some sandstone beds contain low-amplitude bed waves (Baas et al. 2016a; Baker and Baas 2020) (Fig. 11A). A few beds consist of contorted mixed sandstone–mudstone sandwiched between relatively clean, laminated sandstone (e.g., Bed 2e in Fig. 11A).

Unit 4.—Unit 4 consists of thick-bedded and very thick-bedded sandstones and conglomerates, vertically graded from very coarse sand or granules to fine or very fine sand (Figures 7–9, 11B). Mudstone is absent, except for a few thin mudstone beds and occasional mudstone clasts (Fig. 11B). Most sandstones and conglomerates erode into the underlying sandstone (Fig. 11B) and the base of Unit 4 erodes into the underlying Unit 3 (Fig. 7). The visible depth of erosion is up to 1 meter at the base of Unit 4 (Fig. 7) and ranges from several tens to hundreds of millimeters between amalgamated beds in Unit 4 (Fig. 11B). In contrast to the tabular nature of the thick sandstone beds in Unit 3, the sandstones and conglomerates in Unit 4 show lateral variations in thickness and pinch-outs on a scale of tens of meters (Figures 7, 8). The conglomerates lack sedimentary structures, but the sandstones contain massive structureless divisions, plane-parallel stratification, and ripple-cross lamination, often organized in Bouma sequences (e.g., between 3.5 m and 4.6 m on the left-hand log in Fig. 11B), as well as dune cross-bedding, convolute bedding, load casts, and vertical fluid-escape structures (Fig. 11B).

Unit 5.—Unit 5 comprises tabular, predominantly thin-bedded to medium-bedded sandstones interbedded with thin-bedded to thick-bedded mudstones (Figures 7–9). The cumulative mudstone bed thickness is 44% of the total thickness. The sandstone beds are mostly fine-grained or very fine-grained and vertically graded, and they contain variable amounts of mudstone in the matrix (Fig. 12A). Current-induced sedimentary structures in Unit 5 include plane-parallel lamination and ripple cross-lamination, typically organized in incomplete Bouma sequences, and the cross-laminated divisions are often convoluted. This mimics similar beds in Unit 2. In contrast to Unit 2, however, some beds in Unit 5 have massive divisions and the Bouma sequences regularly contain large ripples and low-amplitude bed waves (Baas et al. 2016a, Baker and Baas 2020), rather than “classic” current ripples (Fig. 12A). One bed consists of muddy siltstone with streaks of sandstone sandwiched between plane-parallel-laminated sandstone below and cross-laminated sandstone formed by large ripples above (at 5–30 cm in Fig. 12A).

Unit 6.—Unit 6 consists of tabular, medium-bedded and thick-bedded sandstones and mixed sandstones-mudstones interbedded with thin-bedded and medium-bedded mudstones (Figures 9, 12B). The cumulative mudstone bed thickness is 37% of the total thickness. The maximum grain size in the sandstones ranges from fine sand to very coarse sand. Graded sandstone beds usually start with a massive division overlain by a plane-parallel-laminated division and then a ripple cross-laminated division, thus conforming to the Bouma sequence (Fig. 12B). Convolute bedding and vertical fluid-escape structures are common, and several beds contain divisions with heterolithic sandstone–

mudstone, chaotic mixtures of sandstone and mudstone (e.g., Bed 6b in Fig. 12B), or strongly deformed muddy sandstone (e.g., between 3.4 m and 3.6 m on the right-hand log in Fig. 12B). A few sandstone beds contain low-amplitude bed waves, crude banding, or mudstone clasts.

Interpretation of Lithological Units

Table 1 summarizes the diagnostic properties of the main depositional environments on submarine fans defined by Spychala et al. (2017b), Brooks et al. (2018), and Hansen et al. (2019) and matches these criteria with the observations made in the lithological units in the present study. Below, the lithological units are interpreted following a proximal to distal approach in the submarine system that formed the Aberystwyth Grits Group succession between Aberarth and Llannon.

Unit 4 stands out from the other units by a combination of thick, coarse sandstones and conglomerates, a general lack of mudstone, lateral bed thickness variations, and abundant amalgamation and basal and internal erosion (Table 1), all indicating a high-energy environment. Together with the presence of vertical fluid-escape structures and convolute bedding as well as textural and structural properties that fit the Bouma sequence (Bouma 1962), suggesting rapid deposition from high-density turbidity currents, Unit 4 has been interpreted as a submarine channel fill. This interpretation agrees with the diagnostic properties of channel-fill successions described previously (Table 1). The presence of co-sets of dune cross-bedding in the event beds in the upper half of the channel fill (Fig. 11B) implies that the turbidity currents were sustained for long enough for the dunes to migrate over at least several meters to tens of meters. The lack of mudstone beds and mudstone clasts, and the clean nature of the conglomerates and sandstones in Unit 4, could indicate bypass of fines in the high-density turbidity currents or downdip transport of mud clasts eroded by the heads of these currents.

Unit 2 shows the characteristics of a levee succession (Table 1): (i) thin-bedded, vertically graded, relatively fine-grained sandstones; (ii) dominance of ripple cross-laminated divisions in incomplete Bouma sequences formed by low-density turbidity currents; and (iii) a large amount of mudstone. The ripples in the cross-laminated divisions generally do not climb, so Unit 2 might represent an external levee succession (cf. Kane and Hodgson 2011). The common presence of convolute bedding suggests rapid deposition of sand and postdepositional soft-sediment deformation, possibly by earthquakes in the tectonically active Welsh Basin. Interesting is the occasional presence of low-amplitude bed waves in the turbidites, which implies that some flows were subjected to turbulence attenuation by the presence of cohesive fine particles (Baas et al. 2016a; Baker and Baas 2020). Herein, these deposits are classified as transitional-flow deposits. Further evidence for turbulence attenuation is provided by a few beds with contorted sandstone–mudstone between two relatively clean, laminated sandstones. These beds have been interpreted as hybrid event beds (Haughton et al. 2009, Baas et al. 2011, Fonnesu et al. 2015, 2018), in which the central division resembles a debris-flow deposit. The rare occurrence of hybrid event beds might represent dense superelevated muddy flows that shed the upper part of their sediment load onto the levees, thereby transforming from a turbulent turbidity current to a transitional or laminar hybrid flow upon flow deceleration. Paleocurrents are closely aligned with the overall paleoflow directions of the other units (Fig. 13; Baas 2000), and predominantly in the same orientation as the present-day coastline (Fig. 6). Such flow orientations may represent more distal parts of the external levee (Kane et al. 2010) or the inner external levee (Kane and Hodgson 2011). Alternatively, this may be a fortuitous alignment of higher-angle overbank spillover from a crestal levee area in a more sinuous system (Kane et al. 2010), although the absence of any evidence (e.g., lateral-accretion packages) for sinuous channels in this system, leads us to favor the first interpretation. Unit 2 thus represents the right- or left-lateral spillover deposits of a submarine channel that is not exposed between Aberarth and Llannon.

Units 1, 3, and 7 are poor in mudstone beds, and they also have the coarse-grained texture and the thick event beds in common with the channel-fill succession. However, granule conglomerates, bed amalgamation, and erosion are less pronounced than in Unit 4 and many beds contain evidence for soft-sediment deformation and transitional and laminar flow behavior in the form of convolute and contorted bedding, chaotic mixtures of sandstone and mudstone, mudstone rafts and clasts, and sandstone clasts (Table 1). Most of these beds have been interpreted as hybrid event beds, including varieties described by Fonnesu et al. (2015, 2018) and Pierce et al. (2018). Vertically graded, Bouma-type turbidites, and debris-flow deposits — lacking vertical grading and a basal sandstone — are less common than the hybrid event beds in Units 1, 3, and 7. Vertical dewatering structures, load casts, and foundered sand denote rapid deposition of sediment. Moreover, the load casts and the foundered sand require a sharp vertical density gradient between sand and soft mud or between clean and soft muddy sand. Given the close association with the properties of the channel-fill succession of Unit 4 (Fig. 7) and the location of Unit 3 immediately below this channel fill, Units 1, 3, and 7 have been interpreted as channel–lobe transition zone successions. We infer that the mud and sand eroded in the updip channels were transported by the fast-flowing high-density turbidity currents within the confinement of the channel to the channel–lobe transition zone. Horizontal facies transitions are not exposed in the studied section, but for Unit 3 this could have been the channel that represents Unit 4. Upon arrival in the channel–lobe transition zone, the flows expanded and decelerated, perhaps initially further eroding the substrate. This caused the high-density turbidity currents to transform into transitional and laminar SGFs, as the force balance changed from turbulent forces to cohesive forces (Baas et al. 2011). This transformation may have been helped by the partial disintegration of the mud clasts and rafts eroded from the channel floor, which, together with the presence of softer sand clasts, suggests a short transport distance from the source of erosion in the channel to the channel–lobe transition zone. The SGF deposits in Units 1, 3, and 7 were thicker and the erosional scours were less common than in the channel–lobe transition zone successions described by Brooks et al. (2018) and Hansen et al. (2019). This may indicate that the channels and lobes in the studied part of the Aberystywth Grits Group were not separated by a pronounced zone of bypass and hydraulic jumps (Mutti and Normark 1987; Dorrell et al. 2016; Cunha et al. 2017; Navarro and Arnott 2020). Alternatively, Units 1, 3, and 7 may represent locations in the transition zone that were closer to the lobe than to the channel, where deposition of sediment as hybrid event beds was more important than bypass of sediment (Spychala et al. 2017a, and references therein). It is unlikely that Units 1, 3, and 7 represent submarine lobes, because lobe successions elsewhere in the Aberystwyth Grits Group lack evidence for basal erosion, are finer-grained, contain thinner event beds and thicker background mudstones, and have a higher ratio of turbidites to hybrid event beds (e.g., Baker and Baas, 2020; see also Units 5 and 6 below).

Unit 6 is characterized by tabular, non-erosional and vertically graded sandstones with Bouma sequences, interpreted as deposits of low- and high-density turbidity currents, alternating with tabular, sandy and muddy hybrid beds that contain sandstone divisions and chaotically mixed sandstone–mudstone divisions, the latter also containing mudstone and sandstone clasts. The event beds, therefore, represent a mixture of turbulent and transient-turbulent flows. The inferred transitional flow behavior is further supported by the presence of low-amplitude bed waves in some of the deposits (Baas et al. 2016a; Baker and Baas 2020), classified as transitional-flow deposits (Fig. 14), as in Unit 2. These properties of Unit 6 correspond well with the diagnostic properties of lobe axis and off-axis environments described previously (Table 1). However, it was not possible in the studied section of the Aberystywth Grits Group to distinguish between lobe-axis and off-axis environments, because the event beds straddle thick-bedded T_{abc} turbidites and medium-bedded T_{bc} turbidites (Table 1). Assuming that the coeval channel–lobe transition zone had sedimentological characteristics similar to Units 1, 3, and 7, the lobe deposits lost a large part of the mudstone rafts and mudstone and sandstone clasts present in the updip channel–lobe transition zone. The higher abundance of turbidites in the lobe-axis environment, compared to the channel–lobe transition zone, might indicate that relatively mud-poor, energetic turbidity currents bypassed the channel–lobe transition zone or that hybrid flows transformed into turbidity currents between the channel–lobe transition zone and the lobe-axis (or off-axis) environment.

Unit 5 has the hallmarks of a lobe-fringe succession (Table 1): (i) tabular, non-erosional, thin-bedded to medium-bedded, fine- to very fine-grained sandstones; (ii) current-induced structures in vertically graded beds that are organized into Bouma sequences, thus representing deposits of low-density and some high-density turbidity currents; (iii) a higher cumulative mudstone bed percentage than the lobe-axis (or off-axis) and channel–lobe transition zone successions; and (iv) organization of the event beds in meter-thick sand-rich bed sets. As in most of the other environments, convolute bedding is common, suggesting rapid deposition possibly in a tectonically active setting. The abundance of large ripples and low-amplitude bed waves in mud-rich T_c divisions suggests that the body or tail of the turbidity currents that moved into the lobe fringe environment were turbulence-modulated, possibly as turbulence-enhanced transitional flow and lower transitional plug flow (*sensu* Baas et al. 2011, 2016a), hence their classification as transitional-flow deposits. Unit 5 may represent a frontal fringe environment (Spychala et al. 2017b; Table 1), if the flows lost most of their cohesive load in the coeval channel–lobe transition zone, given the abundance of mud in this more proximal environment and the progressive reduction in transitional-flow and laminar-flow deposits from the channel–lobe transition zone via lobe axis to the lobe fringe. Alternatively, the scarcity of hybrid event beds in Unit 5 may signify deposition in a lateral fringe environment (Spychala et al. 2017b; Table 1). Unit 5 is c. 25 m thick (Fig. 8); such a thick aggradation succession of the lobe fringe facies might be witness to the partially confined nature of the Aberystywth Grits Group basin.

SOLE MARKS

General Observations

A variety of sole marks were found below the SGF deposits in the study area (Table 2). Continuous tool marks are predominately groove marks (Figures 2B, 2D, 15A, 15D, 16A), but chevron marks (Fig. 2C) are also exposed in the coastal cliffs. Discontinuous tool marks include skip marks, tumble marks (Fig. 2D), and skim marks (Fig. 15B), and scour marks comprise symmetric parabolic flute marks (Figures 2A, 15D, 16A), asymmetric parabolic flute marks, and spindle-shaped flute marks (Fig. 15C). Of the 70 SGF deposits investigated, 74% were found to contain a single sole-mark type, 16% comprise flute marks and tool marks or continuous and discontinuous sole marks on the same bed, usually showing crosscutting relationships, and 10% have both parabolic and spindle flute marks, but no tool marks. Beds with crosscutting flute marks and tool marks were most common in the lobe-fringe succession (Unit 5). If tool marks and flute marks crosscut each other, flutes are most often the youngest sole mark (Table 2). According to the model of Peakall et al. (2020), this suggests that the flows that formed the tool marks bypassed the depositional site, before the flutes were formed by a different type of flow. This interpretation is discussed in more detail below. None of the transitional-flow deposits (Fig. 14) contained discernible sole marks.

Of the most common sole-mark types, the groove marks range in width from 5 mm to 250 mm (average: 35 mm) and in depth from 1 mm to 100 mm (average: 20 mm). The largest groove mark was found in channel–lobe transition zone Bed 7a (Fig. 15A). Interestingly, the 0.25 m width of this large groove matched a mudstone clast of similar size found in Bed 7a (Fig. 10C). The skim marks are 1–10 mm wide (average: 7 mm) and 80–280 mm long (average: 153 mm). The flute marks have a large range of sizes, with the largest flutes occurring in the channel-fill succession (Fig. 2A). The parabolic flutes range in width from 10 mm to 700 mm (average: 90 mm), in length from 40 mm to 710 mm (average: 159 mm), and in depth from 10 mm to 80 mm (average: 33 mm). The spindle flutes are generally smaller than the parabolic flutes; their width, length, and depth are 10–80 mm (average: 23 mm), 40–700 mm (average: 138 mm), and 10–30 mm (average: 17 mm), respectively. The size of these types of scour and tool mark agrees with their typical size distribution mentioned in the literature (Peakall et al. 2020).

Relating Sole Marks to Bed Type

Beds with Bouma-type sequences of sedimentary structures in the study area were interpreted as turbidites. These turbidites were subdivided into high- and low-density turbidity-current deposits, based on the presence or absence of a massive, structureless basal T_a division. Figure 16A shows that most turbidites are associated with flute marks, but no relationship between low-density or high-density turbidity-current deposits and parabolic or spindle flutes was apparent. A small number of tool marks was also found below these event beds, either alone or in combination with flutes (Table 2).

Event beds that show evidence for an internal flow fabric, usually in the form of sandstone and mudstone clasts floating in a chaotic muddy or mixed sand–mud matrix, and lack vertical grading and a basal sandstone division, were interpreted as debris-flow deposits. These debrites were confined to the channel–lobe transition zones, where they were associated exclusively with groove marks (Fig. 16A, Table 2).

The relationship between hybrid event beds and sole-mark types shown in Fig. 16A is based on a broad definition of hybrid event beds that goes beyond the five-division hybrid-event-bed model originally proposed by Haughton et al. (2009). Most beds match the principal organization of a muddy or mixed sandstone–mudstone H3 division sandwiched between sandy divisions (H1 divisions and H4 divisions; H2 banded divisions are uncommon) of Haughton et al. (2009) and Fonnesu et al. (2018), such as the three beds at 2.4–3.7 m in the log of Unit 1 (Fig. 10A), Bed 2e (Fig. 11A), Bed 3c (Fig. 10B), the 0.26-m-thick bed at the base of the log of Unit 5 (Fig. 12A), and Bed 6c (Fig. 12B). However, the H1 division is often atypical of Haughton et al. (2009)'s model in that it may contain plane-parallel lamination (e.g., Bed 2e [Fig. 11A], and the bed at the base of the log of Unit 5 [Fig. 12A] and at 4.8–5.0 m in the log of Unit 6 [Fig. 12B]). In other beds, the H1 division is absent and only a banded H2 division is present below the H3 division (Bed 6c in Fig. 12B and Bed 7d in Fig. 10C). This presence of primary current stratification in H1 divisions of hybrid event beds tallies with similar observations by Baker and Baas (2020) in a lobe-fringe and distal-lobe-fringe environment further downdip in the Aberystwyth Grits Group deep-water fan system, as also observed in some other systems (e.g., "crude lamination" of Fonnesu et al. 2018; in lowermost division of the HEB3 hybrid event beds of Pierce et al. 2018). Moreover, in half of the hybrid event beds the H4 divisions are either missing (e.g., Beds 1d and 3d in Fig. 10, and Bed 6d in Fig. 12B) or unusually thick (e.g., Bed 6c in Fig. 12B and Bed 7b in Fig. 10C). These departures from the classic hybrid-event-bed model — and the model extension proposed by Fonnesu et al. (2018) — suggest that the hybrid event beds in the study area were not merely the result of deposition from a forerunner high-density current followed by deposition from a debris flow with a dilute turbulent wake. More complex spatio-temporal changes in flow behavior took place, possibly driven by a combination of processes that modified the balance between cohesive and turbulent forces in different ways. These processes might include flow confinement and expansion, horizontal fractionation and vertical segregation of sand and clay, erosion of substrate mud, and disaggregation of mud clasts and rafts. Fully disentangling the role of these processes is difficult without further research, including the application of novel microscopic and geochemical methods proposed by Hussain et al. (2020), who, like Baker and Baas (2020), found that H1 divisions in hybrid event beds can be formed by transitional flows. However, the presence of large ripples, low-amplitude bed waves, grain-size banding, ubiquitous soft-sediment deformation structures, and clearly separated basal sandstone from mixed sandstone–mudstone suggest that turbulence-modulated, transitional flows (*sensu* Baas et al. 2009, 2011) may have played an important role in sediment transport in the basin. Thus, the H1 divisions may represent not only high-density turbidity currents, but also low-density turbidity currents in the presence of plane-parallel lamination, and transitional flows in the presence of grain-size banding, large ripples, and low-amplitude bed waves (Lowe and Guy 2000; Baas et al. 2011, 2016a; Stevenson et al. 2020). The missing H4 divisions are inferred to indicate a stable, stratified debris flow without significant upper-boundary mixing with ambient water (cf. Talling et al. 2002; Baker et al. 2017) or postdepositional loading of the H4 sand and silt into the underlying H3 division. The latter process explains the common occurrence of sand clasts and ball-and-pillow structures in the hybrid event beds. Finally, the thick H4 and H5 divisions may indicate that large amounts of sand were kept in suspension by turbulence in late-stage, relatively clay-poor, low-density and high-density turbidity currents. The presence of massive and laminated divisions in these thick H4 divisions (Beds 6c and 7e) supports this interpretation.

Figure 16A reveals that most hybrid event beds are associated with continuous tool marks, i.e., groove marks, with a subordinate amount of discontinuous tool marks, i.e., skim marks, also found below these event beds. Flute marks are rare below hybrid event beds. Several hybrid event beds in the study area were subdivided into muddy and sandy varieties (Table 2), referring to the dominant grain size in the H3 division. However, no consistent relationships between sole-mark type and hybrid-event-bed variety were found.

Relating Sole Marks to Lower Divisions of Event Beds

Considering the complex internal organization of the hybrid event beds described above and the fact that intuitively sole-mark types are most likely coupled with the part of flows that form the lower division in event beds, Fig. 16B shows the relationship between sole-mark type and lower-division type. These include ripple cross-laminated, plane-parallel laminated, banded, massive, and debritic divisions. Debritic and banded lower divisions are associated exclusively with continuous tool marks, i.e., groove marks. The debritic divisions are present in debrites and hybrid event beds, whereas the banded divisions were found only in hybrid event beds. Plane-parallel-laminated and ripple-cross-laminated divisions are coupled mainly with flute marks (Fig. 16B) below turbidites, with a quarter of current-laminated lower divisions in turbidites and hybrid event beds exhibiting grooves. Massive divisions were found to contain a wider range of sole-mark types, but continuous sole marks make up the majority (Fig. 16B). The flutes were all present below massive T_a divisions in deposits of high-density turbidity currents, whilst the groove marks and skim marks are associated with massive basal divisions in both hybrid event beds and turbidites.

Relating Sole Marks to Depositional Environment

Figure 17 summarizes the frequency distribution of main tool-mark types and event-bed types for the various depositional environments. The event-bed types include turbidites, debrites, hybrid event beds, and beds dominated by low-amplitude bed waves and large ripples (e.g., Fig. 14, at 3 m in the log of Unit 2 [Fig. 11A], at various heights in the log of Unit 5 [Fig. 12A], and at 1 m in the log of Unit 6 [Fig. 12B]), which have been interpreted as the product of flows with transitional turbulent–laminar behavior (Baas et al. 2011, 2016; Baker and Baas 2020). The channel and levee environments are dominated by flute marks below deposits of high-density and low-density turbidity currents, respectively (Fig. 17; Table 2). No preference for parabolic or spindle flutes was found in these environments. The single bed with skim marks in the levee succession was a hybrid event bed, whilst two other hybrid event beds contained flute marks. Hybrid event beds make a sudden appearance in the channel–lobe transition zone, accompanied by a rapid increase in the proportion of tool marks. The transect from channel–lobe transition zone via axial lobe (or off-axis) to lobe fringe reveals an increase in the frequency of turbidites and transitional-flow deposits at the expense of hybrid event beds, mirrored by an increase in flume-mark frequency and a decrease in continuous-tool-mark frequency, respectively. The data in Table 2 show that these mirror-image relationships are not confounded by other factors; only 13% of the beds lack a one-to-one relationship between turbidites and flute marks and between hybrid event beds and groove marks. Discontinuous sole marks, i.e., skim marks, constitute a small proportion of the total sole-mark population in the channel–lobe transition zone and the lobe-axis (or off-axis) environments, but skim marks are absent from the lobe-fringe environment. Debrites with groove marks are confined to the channel–lobe transition zones. None of the transitional-flow deposits contained discernible sole marks.

USING SOLE MARKS TO RECONSTRUCT DEPOSITIONAL PROCESSES AND ENVIRONMENTS

General Remarks

The environmental distribution of the sole marks and the event beds in the study area match remarkably well. Together with the strong relationship between the sole marks and the lower divisions of event beds, summarized in Figures 16 and 17, this allowed us to test if and how the field data agree with the model of Peakall et al. (2020) and add this new information to the reconstruction of the deep-marine system in the Aberystwyth Grits Group between Aberarth and Llannon, with a focus on the flow mechanics and depositional products of hybrid events.

Comparison with Peakall et al. (2020)

Flute Marks below Turbidites.—The strong relationship between flute marks and turbidites found in the study area agrees well with the model prediction of Peakall et al. (2020) that turbulent shear flows are required to form flute marks, but the proposed downslope change from small via large parabolic flutes to small spindle flutes (Fig. 1) cannot be verified in this particular case. Linking large ripples to flume-mark type may achieve this, because the change from small to large parabolic flutes requires a change from turbulent to turbulence-enhanced transitional flow, and large ripples form below turbulence-enhanced transitional flow (Baas et al. 2016a). However, transitional-flow deposits with both large ripples and sole marks have not been found in the study area. An increase in turbulence intensity could also be achieved by an increase in flow velocity, so that faster turbidity currents, e.g., high-density turbidity currents that form turbidites with T_a divisions, are more likely to have large parabolic flutes than small parabolic and spindle flutes (Allen 1971). The field data show that both T_{abc} beds and T_b-beds have a clear preference for parabolic flutes, occasionally together with spindle flutes on the same surface. A larger percentage of T_{bc} beds and T_c beds than T_{abc} beds have spindle flutes (in agreement with Pett and Walker 1971), but this difference is small. However, the above-mentioned rapid deceleration of turbidity currents upon lateral expansion in the channel–lobe transition zone and on the levee, and the more gradual deceleration when the flows travel on the lobe, is mimicked by similar trends in mean length and depth of flutes (Fig. 18AB), suggesting that a predictable relationship exists between flume-mark size and flow velocity and turbulence intensity. Based on defect-theory modelling by Allen (1971), Peakall et al. (2020) suggested that surfaces with flute marks change in a downstream direction from conjugate to isolated. Some supportive evidence was found in the study area, where the ratio of event beds with conjugated to isolated flutes changes from 100% in the channel via 50% in the lobe axis (or off-axis) to 33% in the lobe-fringe environment, but event beds on the levee are also dominated by conjugated flutes.

Tool marks below turbidites.—Tool marks below turbidites were found mainly beneath deposits of high-density turbidity currents downstream of channel terminations, suggesting that at least some tools bypassed the channel–lobe transition zone and the lobe hin debris flows or upper transitional plug flows. It is unclear if these turbulence-attenuated flows were part of the same event that also formed the high-density turbidity current deposits overlying the tool marks or if these were separate events.

Groove Marks below Debris-Flow Deposits.—The debris-flow deposits in the study area are associated exclusively with groove marks (Fig. 16). This relationship is correctly predicted by the model of Peakall et al. (2020), indicating that dense, laminar flows transport tools that are in continuous contact with the bed and do not rotate during downstream movement (Fig. 1).

Discontinuous Tool Marks below Hybrid Event Beds.—Skim marks are most common below hybrid event beds and massive divisions in other event beds. Figure 1 implies that these discontinuous tool marks were generated by upper transitional plug flow, which is supported implicitly by: (i) the presence of the skim marks below massive sandstone divisions, since Baas et al. (2011) found massive sand at the base of deposits generated by upper transitional plug flows; and (ii) the occurrence of the skim marks in the levee, channel–lobe transition zone, and lobe-axis (or off-axis) environments, where decelerated flow, as a result of lateral flow expansion, is most likely to occur. However, the small number of discontinuous tool marks between Aberarth and Llannon (Table 2) prevents us from making more detailed inferences about the relationship between discontinuous tool mark and transitional flow type (Fig. 1). Under laboratory conditions, lower and upper transitional plug flows were stable at a narrow range of clay concentrations of c. 4 vol% (Figure 15 of Baas et al. 2009), compared to turbulent and laminar flows. This might explain why flutes and grooves, formed by turbulent and laminar flow, respectively (Fig. 1), are more common than discontinuous tools in the study area. Further research in other deep-marine systems is needed to validate this supposition.

Groove Marks below Hybrid Event Beds.—Groove marks are the most common sole-mark type underneath hybrid event beds in the study area (Fig. 16A). The model of Peakall et al. (2020) predicts that the SGFs that generated these tool marks were predominately of high internal strength and laminar or quasi-laminar in kinematic behavior. Independent support for this non-turbulent flow behavior is the remarkably constant cross-sectional shape and internal structure of the observed grooves over distances on the scale of meters to occasionally tens of meters, which would be difficult to achieve in transient-turbulent and fully turbulent flow. However, this inferred highly cohesive flow behavior needed to keep clasts in a fixed position whilst being dragged along the bed disagrees with the hybrid-event-bed model of Haughton et al. (2009), in which the massive H1 division represents a high-density turbidity current. Above, it was argued that the H1 division can in other cases form from turbulent flow and transitional flow, supported by the presence of flute marks and skim marks at the bases of some hybrid event beds (Fig. 16). A detailed explanation for the formation of groove marks at the bases of the hybrid event beds is provided in the section *A new process model for hybrid event beds* below.

Longitudinal Distribution of Flute and Tool Marks.—Peakall et al. (2020; their Figure 24B) proposed a downdip distribution of sole marks based on transformation from turbulent to cohesive flow (Fig. 1) and from cohesive to turbulent flow, in which the sequence of sole-mark types is the reverse of that shown in Fig. 1. The Aberystwyth Grits Group data show that the spatial distribution of sole marks can be more complex, if the flow-lateral dimension is added to the model. The reverse of the model shown in Fig. 1 can be used to describe the changes in sole-mark type from the channel–lobe transition zone to the lobe fringe. However, the change from groove marks to flute marks along this transect is related to flow type in a more complex manner. The increasing dominance of turbidity currents described above is not related to the transformation of single flows from debris flow and transitional flow to turbidity current. Instead, relatively clay-poor turbidity currents emanating from the channel kept enough momentum to bypass the channel–lobe transition zone and the lobe-axis (or off-axis) environment. Turbidity currents charged with clay, on the other hand, transformed into hybrid flows, transitional flows, and debris flows upon flow deceleration in the channel–lobe transition zone and only the most mobile of these flows made it onto the lobe. This process thus matches the flow-transformation model portrayed in Fig. 1. This contrasting behavior of the turbidity currents at the mouth of the channel caused the channel–lobe transition zone and the lobe environment to record a mixture of different sole marks. Yet, the type of sole mark was still closely linked to flow type (Fig. 17), which is used below to propose a new process model for hybrid event beds.

Type and Source of Tools.—Peakall et al. (2020) stated that intra-basinal mudstone clasts are the most likely tools to form tool marks. Our field observations agree with this statement, considering that mudstone (and sandstone) clasts are abundant in the channel–lobe transition zone and the lobe axis (or off-axis) environment, and the channel floor is most likely the main source of these clasts.

Evidence for Bypassing Flows from Tool Marks.—Peakall et al. (2020) further stated that both flute marks and tool marks can be present below deposits of high- and low-density turbidity currents. This is supported by the presence of grooves, skim marks, and a tumble mark below T_{bc}-bed 5e (Fig. 2D), and grooves below, for example, T_{ab}-bed 6a. Peakall et al. (2020) interpreted the presence of tool marks below turbidites as evidence for bypassing flow. The lobe-fringe succession shows the largest number of beds with crosscutting flute marks and tool marks. Flute marks cut into grooves and other tool marks underneath Beds 5a, 5b, and 5c, whilst grooves are the youngest tool mark below Beds 5d and 5e, as they cut into other tool marks (Table 2). Based on these crosscutting relationships, the model of Peakall et al. (2020) predicts that debris flows and hybrid flows bypassed the lobe fringe before turbidity currents formed flutes and Bouma-type turbidites. This is in contrast with the above-mentioned interpretation that only the most mobile turbulence-attenuated transitional flows made it onto the lobe. However, it does agree with the discovery of Baker and Baas (2020) of hybrid event beds and transitional-flow deposits with large ripples and low-amplitude bed waves on the lobe fringe and distal fringe in a more distal location of the Aberystwyth Grits Group deep-marine system (c. 16 km north of Llannon). Given the common occurrence of groove marks downdip of the mouth of the submarine channel, these tool marks may be associated with laminar, high-concentration, clay-rich heads of hybrid flows with mud clasts that bypassed most of the fan towards the distal lobe fringe, as explained in more detail next.

A NEW PROCESS MODEL FOR HYBRID EVENT BEDS

Rationale

The observation in the study area of groove marks immediately below hybrid event beds, coupled with the reduced proportion of hybrid event beds in the lobe compared to the channel–lobe transition zones and the concurrent reduced proportion of groove marks associated with these hybrid event beds, suggests that in these cases: i) groove formation is intrinsic to the development and deposition of hybrid event beds; or ii) the grooves were cut by previous flows, and later hybrid event beds were deposited on top of these surfaces. The latter interpretation can be discounted because it is hard to envisage how bypassing debris flows that travelled beyond the hybrid event beds in the channel–lobe transition zone would be associated with a rapid decrease in the number of grooved surfaces towards the lobe axis (or off-axis) and lobe fringe without forming debris-flow deposits. Furthermore, it is unclear why the beds overlying the grooved surfaces are so frequently hybrid event beds if these are not genetically related, given that hybrid event beds constitute only a subset of all possible flow types. Present hybrid-event-bed models (Haughton et al. 2003, 2009; Talling et al. 2004; Fonnesu et al. 2016; Kane et al. 2017) do not explain how groove marks can be found directly underneath hybrid event beds (Peakall et al. 2020). Furthermore, for a flow that erodes mud clasts to produce a debritic division, these models do not explain the process mechanics responsible for forming the debritic H3 division. Herein, we examine the nature of erosion by and the temporal development of hybrid flows such as those inferred for the studied channel-to-lobe system of the Aberystywth Grits Group (Figures 19 and 20). Figures 19A and 19B discriminate the bypassing head and depositional body of the hybrid flows, respectively. For the sake of completeness, Figures 19C and 19D show the temporal development of the transitional flows and turbidity currents.

Erosion at the Head

In the study area, turbidity currents eroded the submarine channel floor down to a depth of at least one meter (Fig. 19A). The applied bed shear stresses are greatest in the head of turbulent gravity currents (Necker et al. 2002). Therefore, erosion of both unconsolidated mud and mud clasts likely takes place primarily below the head. Erosion beneath the head of a turbidity current has also been inferred in Late Quaternary hybrid event beds on the East China Sea Shelf where localized erosion is indicated by the presence of distinctive locally sourced mud clasts (with distinct $\delta^{13}C$ values) in the resultant H1 division (Shan et al. 2019a, 2019b). Sustained erosion below the head then leads to increased flow density and cohesivity, with the latter primarily the result of the incorporation of weak substrate mud. Monitoring of flows in the mud-dominated Congo submarine channel has revealed a high-concentration "flow cell" at the front of the head which was linked to the entrainment of seafloor sediment (Azpiroz-Zabala et al. 2017). These Congo data suggest that in mud-rich systems only a small part of the head undergoes rapid flow bulking through erosion. This inference is supported by the flume experiments of Sequeiros et al. (2009, 2018), which show that preferential erosion below the head causes the head to become denser. These experiments have also shown that this process may initially be self-reinforcing, as the incorporation of sediment into the head leads to stronger velocity fluctuations that might be expected to lead to stronger turbulence and thus increased erosion (Sequeiros et al. 2018), possibly related to the formation of turbulence-enhanced transitional flow (Baas et al. 2009). It is postulated herein, following Kane et al. (2017), that the frontal "flow cell", or perhaps the whole head, can transform into a debris flow if the erosion is continuous (Figures 19A, 20). At this point, the larger clasts are supported by the high strength of the cohesive mass, thus able to cut grooves (Peakall et al. 2020) beneath the head. This scenario explains the spatial distribution of the groove marks and their dominant relationship with hybrid event beds in the channel–lobe transition zone (Figures 19A, 20). The proposition that grooves are cut under only a limited longitudinal part of the flow also explains the observation that groove marks are typically preserved in a pristine form, rather than repeatedly cut and eroded by subsequent groove marks (Peakall et al. 2020). Peakall et al. (2020) suggested that outsized clasts towards the front of the flow are a likely answer to this conundrum, as proposed in the hybrid-event-bed model presented here (Fig. 20).

Longitudinal Segregation of Bedload

During the erosive phase in the channel, whilst the flow front is not yet cohesive enough to support the eroded mud clasts in a debris flow, the mud clasts move as bedload. Bedload sediment travels slower than suspended sediment, with the velocity of clasts decreasing as a function of increasing grain diameter (e.g., Bridge and Dominic 1984). Therefore, the mud clasts move backwards relative to the head, with the smallest mud clasts (sub-mm to mm in diameter; Stevenson et al. 2020) moving fastest, presumably via saltation, whilst the larger clasts undergo segregation as a function of size, as well as angularity, during bedload transport (Fig. 20).

Vertical Segregation of Suspended Load

As the flow decelerates across a given point in the channel–lobe transition zone, segregation of the mixed sand–mud suspension begins to occur in the body of the flow, with sand settling out of the mud suspension and aggrading to form the H1 division of the hybrid event bed (Baas et al. 2011) (Figures 19B, 20). This flow deceleration also leads to a decrease in turbulence intensity and thus a relative increase in the cohesivity of the flow, possibly helped by the removal of the sand from suspension. If the flow decelerates at a moderate rate, the increased cohesivity may result in the formation of banding in the form of low-amplitude bed waves in a H2 division (Baas et al. 2011, 2016a; Stevenson et al. 2020) (Figures 19B, 20). Yet, H2 divisions were rare in the study area, supporting the above-mentioned evidence that the flows in the study area decelerated rapidly when emanating from the channel mouth. Given further increases in cohesivity, a mud-rich debritic unit forms, representing the H3 division of the hybrid event bed (Figures 19B, 20). Whilst the H3 division cannot be subdivided based on the available field data in the Aberystywth Grits Group, Hussain et al. (2020) have shown, using high-resolution X-ray fluorescence core scanning, that this division can often be subdivided into H3a divisions and H3b divisions. The H3a division shows some segregation and stratification of the remaining sand fraction, whereas the H3b division is a true debris flow without segregation of sand (Hussain et al. 2020). Taken together, this sequence represents a progressive increase in cohesivity as a result of vertical segregation of the suspended load, in response to deceleration producing increasing cohesion throughout the depositional process in the hybrid event bed (Baas et al. 2011) (Figures 19B, 20). Progressive disintegration of the mud clasts in the hybrid event may enhance the process of increasing cohesivity during the formation of the H1, H2 and H3 divisions.

Interaction of Longitudinal and Vertical Segregation Processes (H1–H3 Divisions)

The nature of the H1–H3 divisions depends on the interaction of the segregation processes associated with the bedload (longitudinal segregation) and suspension load (vertical segregation). The bedload fraction moves across the basal substrate while the flow is bypassing. As the flow decelerates, vertical segregation commences, and the H1 division starts to aggrade (Figures 19B, 20). Most of the bedload will bypass the top of this solid aggrading surface, but isolated clasts can be incorporated into the aggrading H1 division (Fig. 20), as observed in the hybrid event beds in the study area — either as randomly distributed clasts, as clasts near the base of the H1 division, or concentrated along horizons — and in previous work (Haughton et al. 2009; Shan et al. 2019a, 2019b). This gradual aggradation matches the aforementioned sustained nature of the SGFs, inferred from the presence of migrating dunes in the submarine-channel fill. Where present, the H2 division represents bedform development under slow to moderately decelerating flows in the lower or upper transitional plug-flow regimes (Baas et al. 2011, 2016a; Stevenson et al. 2020). Such banded layers frequently incorporate large numbers of small mud clasts, representing the fastest moving part of the bedload component closest to the head of the flow. As the flow further increases in cohesivity, buoyant forces become important, and the bedload fraction starts to be incorporated into high-strength transitional flows where minor segregation can still occur (H3a), then into a true debris flow (H3b) (Figures 19B, 20). The mud clasts not incorporated into the H2 division, thus dominantly the larger slower-moving mud clasts, are incorporated into the H3b division which flows as a debris flow before depositing en masse. The late-stage formation of this debris-flow component is in keeping with the typically thin (average: 0.15–0.20 m) H3 divisions in the Aberystywth Grits Group between Aberarth and Llannon. In other deposits, the debritic component was observed to extend beyond the underlying sandstone (Spychala et al. 2017b). However, this aspect is not included in the model here, because it is not clear if this is related to hybrid event beds associated with rapid increases in cohesion (Spychala et al. 2017b). In the present examples such thin debritic flows are unlikely to travel far independently (e.g., Figure 9c of Talling, 2013).

Formation of the Sandy H4 Division and the Muddy H5 Division

The sandy H4 division is inferred to form in one of two ways. This division may represent another longitudinally segregated flow component, driven by mixing at the top of the flow, producing dilute, slow-moving fluid that becomes the tail of the flow, and thus being deposited last as a thin capping sand. However, in several examples in the study area and elsewhere (e.g., Hussain et al. 2020) thick H4 divisions were observed. It is hard to envisage how such thick H4 divisions can represent the tail of the flow resulting from longitudinal segregation. These thick H4 divisions may instead represent continued turbiditic input that was sufficiently far behind the erosive flow front that it did not incorporate significant additional unconsolidated mud or mud clasts (Fig. 20). The overlying H5 division is envisaged to form by longitudinal segregation, given sufficient flow duration, as a result of the low velocities at the top of the flow (Kneller and McCaffrey 2003).

Absence of a Forerunning Turbidity Current

The classic Haughton et al. (2003, 2009) hybrid-event-bed model invokes a forerunning turbidity current. We have argued herein that the field observations, including the presence of groove marks, indicate that the front of the flow that formed each hybrid event bed was a debris flow. The reason that the turbiditic component does not simply outrun the debris-flow head may be that erosion in the head causes the head to become denser and faster, therefore producing local self-acceleration of the flow, as shown experimentally (Sequeiros et al. 2009, 2018). Similarly, erosion of a weak surficial-mud layer has been postulated as the likely mechanism for the acceleration of a turbidity current in Monterey Canyon (Heerema et al. 2020; cf. Wang et al. 2020), and, as noted above, the fastest part of the Congo flows was the “flow cell” at the front of the flow (Azpiroz-Zabala et al. 2017). In such situations, the debritic head moves faster than the following turbidity current. Self-acceleration *sensu* Sequeiros et al. (2009, 2018) has been recorded only in supercritical flows, which are most likely found on steeper slopes and in smaller basins, such as postulated for the Aberystywth Grits Group. In examples where the flows traverse extensive flat areas of seafloor, any initial debritic head developed through substrate erosion is likely to be overtaken by the turbiditic component to produce the forerunning turbidity current of the Haughton et al. (2003, 2009) model. These contrasting scenarios of longitudinal segregation of flow components may also be recorded in the crosscutting mode of flute marks and groove marks. With a debritic head like that postulated herein for the Aberystywth Grits Group, grooves should be cut by flutes, whereas flutes should be cut by grooves in examples with a forerunning turbidity current. Consequently, the crosscutting relationships of flutes and grooves might indicate the longitudinal structure of the flow that produced the hybrid event bed. In the study area, the debritic-head model is supported by the observation that flute marks are most often the youngest sole mark below beds with crosscutting tool marks and flute marks.

Where is the Debritic Head?

No deposits from debritic heads were observed in the Aberystywth Grits Group between Aberarth and Llannon, nor in other studies that predict a debritic component updip (Kane et al. 2017). It is proposed here that, once the flow ceases to entrain additional substrate sediment, mixing with ambient water (Talling et al. 2002; Felix and Peakall 2006), and possibly hydroplaning and injection of fluid into the base of the flow (Hampton 1970; Mohrig et al. 1998), start to dominate the front of the flow (Fig. 19A).

Such mixing is shown schematically in the Kane et al. (2017) model (their Figure 18). Kane et al. (2017) argued that segregation of the original debris flow can then occur. Once flow strength is lost, the remaining mud clasts become bedload, and travel more slowly than the flow front, as discussed above. Interestingly, the "flow cell" observed in the Congo flows (Azpiroz-Zabala et al. 2017), being such a small component of the head, suggests that the development and subsequent dissipation of a debris-flow component at the front of a flow may be comparatively rapid. This dissipation process helps explain the rapid change from groove marks to flute marks from the channel–lobe transition via the lobe axis (or off-axis) to the lobe fringe in the study area (Fig. 19A).

Comparison with Existing Hybrid-Event-Bed Models

There has been much debate as to whether a longitudinal segregation model (e.g., Haughton et al. 2003, 2009), or a vertical segregation model (Baas et al. 2011) is the correct description for hybrid event beds. Here, based on the development of a model that explains the field observations in the Aberystywth Grits Group, it is suggested that both are required. In particular, the model separates bedload and suspension-load processes that undergo longitudinal and vertical segregation in the H1–H3 divisions, respectively. The present model also explains how the debritic H3 division develops from the initial erosion of mud clasts through to their final incorporation into the debritic unit. The model postulated here explains the conundrum of how anomalously thin debritic layers (e.g., 100s of millimeters thick) can be transported over apparently long distances as is implicit in hybrid-event-bed models with purely longitudinal segregation. The present model suggests that such long-distance transport of thin debris flows need not occur; rather, the debris flows are formed as a relatively late-stage process via vertical segregation.

CONCLUSIONS

The present field study in the Aberystwyth Grits Group has revealed predictable relationships between sole-mark type and size and depositional process that agree well with the model of Peakall et al. (2020). Turbidites, i.e., the products of *turbulent* gravity flows, are mainly associated with flute marks, whereas groove marks dominate the deposits of debris flows, i.e., flows with *laminar* behavior. Discontinuous tool marks are less common than continuous tool marks and scour marks in the study area. The available field data, therefore, did not allow us to test the detailed relationships between discontinuous-tool-mark type and transitional-flow type proposed by Peakall et al. (2020). Vertically stacked event-bed sequences in the study area were interpreted as submarine channels, levees, channel–lobe transition zones, lobe axes (or off-axes) and lobe fringes. Each of these environments has a unique assemblage of sedimentary facies and sole marks, thus inspiring confidence that sole marks can be used more widely to aid facies analysis and architectural analysis in other deep-marine sedimentary systems. Specifically, turbidites with flute marks dominate the channel-fill and levee units, whereas flute marks below turbidites increase in frequency at the expense of groove marks below hybrid event beds in a downstream direction from the channel–lobe transition zone via the lobe axis (or off-axis) to the lobe fringe. Evidence for bypassing flows from a mismatch between sole-mark type and event-bed type (or lower-division type) is rare, other than for groove marks below massive H1 divisions of hybrid event beds. Because H1 divisions are unlikely to be generated by debris flows, a new model for the mechanics of hybrid flows is proposed. This model involves a bypassing debris flow that is formed by erosion of clay from the channel floor by turbidity currents and rapid flow deceleration and flow transformation in the channel–lobe transition zone. This debris flow is confined to the head of the hybrid flow and forms grooves downstream of the channel mouth. Behind the head, a combination of longitudinal segregation of bedload and vertical segregation of suspension load is used to interpret the formation of the H1, H2, and H3 divisions of hybrid event beds. This process involves a progressive increase in cohesivity in the body of the hybrid event. The debritic head of the hybrid flow is postulated to transform in a downstream direction into a turbidity current, following cessation of seabed erosion and progressive admixture of ambient water. Further work beyond the Aberystwyth Grits Group is needed to determine if this model has a generic place alongside the Haughton et al. (2009) model for the development of hybrid event beds. This study demonstrates that sole marks can be an integral part of sedimentological studies at different scales, thus beyond their traditional use as paleoflow direction or orientation indicators.

ACKNOWLEDGMENTS

The authors would like to thank Guy Springett, David Roberts, and Peter Valender for their help in collecting and processing the field data. Michele and John Tracey are acknowledged for their support during write-up. This project was partly funded by a grant from Equinor Norway. We are grateful to Dave Lee for helping with several figures. The 3D point-cloud models of the outcrop are available upon request from the corresponding author. We thank Yvonne Spychala and Peter Haughton, along with Associate Editor Joris Eggenhuisen and Science Editor Kathleen Marsaglia, for their detailed reviews and comments.

REFERENCES

Allen, J.R.L., 1968, Flute marks and flow separation: Nature, v. 219, p. 602–604.

Allen, J.R.L., 1971, Transverse erosional marks of mud and rock: Their physical basis and geological significance: Sedimentary Geology, v. 5, p. 167–385.

Allen, J.R.L., 1984, Sedimentary Structures: Their Character and Physical Basis: Amsterdam, Elsevier, 1256 p.

Azpiroz-Zabala, M., Cartigny, M.J.B., Talling, P.J., Parsons, D.R., Sumner, E.J., Clare, M.A., Simmons, S.M., Cooper, C., and Pope, E.L., 2017, Newly recognized turbidity current structure can explain prolonged flushing of submarine canyons: Science Advances, v. 3, doi.org/10.1126/sciadv.1700200.

Baas, J.H., 2000, EZ-ROSE: A computer program for equal-area circular histograms and statistical analysis of two-dimensional vectorial data: Computers & Geosciences, v. 26, p. 153–166.

Baas, J.H., Best, J.L., Peakall, J., and Wang, M., 2009, A phase diagram for turbulent, transitional, and laminar clay suspension flows: Journal of Sedimentary Research, v. 79, p. 162–183.

Baas, J.H., Best, J.L., and Peakall, J., 2011, Depositional processes, bedform development and hybrid flows in rapidly decelerated cohesive (mud–sand) sediment flows: Sedimentology, v. 58, p. 1953–1987.

Baas, J.H., Best, J.L., and Peakall, J., 2016a, Predicting bedforms and primary current stratification in cohesive mixtures of mud and sand: Geological Society of London, Journal, v. 173, p. 12–45.

Baas, J.H., Best, J.L., and Peakall, J., 2016b, Comparing the transitional behaviour of kaolinite and bentonite suspension flows: Earth Surface Processes and Landforms, v. 41, p. 1911–1921.

Baker, M.L., and Baas, J.H., 2020, Mixed sand–mud bedforms produced by transient turbulent flows in the fringe of submarine fans: Indicators of flow transformation: Sedimentology, v. 67, p. 2645–2671.

Baker, M.L., Baas, J.H., Malarkey, J., Silva Jacinto, R., Craig, M.J., Kane, I.A., and Barker, S., 2017, The effect of clay type on the properties of cohesive sediment gravity flows and their deposits: Journal of Sedimentary Research, v. 87, p. 1176–1195.

Bouma, A., 1962, Sedimentology of some Flysch Deposits: A Graphic Approach to Facies Interpretation: Amsterdam/New York, Elsevier, 168 p.

Bridge, J.S., and Dominic, D.F., 1984, Bed load grain velocities and sediment transport rates: Water Resources Research, v. 20, p. 476–2490.

Brooks, H.B., Hodgson, D.M., Brunt, R.L., Peakall, J., Hofstra, M., and Flint, S.S., 2018, Deep-water channel–lobe transition zone dynamics: processes and depositional architecture, an example from the Karoo Basin, South Africa: Geological Society of America, Bulletin, v. 130, p. 1723–1746.

Cherns, L., Robin, M., Cocks, L., Davies, J., Hillier, R.A., Waters, R., and Williams, M., 2006, Silurian: The influence of extensional tectonics and sea-level changes on sedimentation in the Welsh Basin and on the Midland Platform, *in* Brenchley, P.J., and Rawson, P.F., The Geology of England and Wales: The Geological Society of London, p. 75–102.

Collinson, J., and Mountney, N., 2019, Sedimentary Structures: Edinburgh, Dunedin Academic Press, 340 p.

Craig, G.Y., and Walton, E.K., 1962, Sedimentary structures and palaeocurrent directions from the Silurian rocks of Kirkcudbrightshire: Edinburgh Geological Society, Transactions, v. 19, p. 100–119.

Cunha, R.S., Tinterri, R., and Muzzi Magalhaes, P., 2017, Annot Sandstone in the Peïra Cava basin: An example of an asymmetric facies distribution in a confined turbidite system (SE France): Marine and Petroleum Geology, v. 87, p. 60–79.

Dirnerová, D., and Janočko, J., 2014, Sole structures as a tool for depositional environment interpretation: a case study from the Oligocene Cergowa Sandstone, Dukla Unit (Outer Carpathians, Slovakia): Geological Quarterly, v. 58, p. 41–50.

Dorrell, R.M., Peakall, J., Sumner, E.J., Parsons, D.R., Darby, S.E., Wynn, R.B., Özsoy, E., and Tezcan, D., 2016, Flow dynamics and mixing processes in hydraulic jump arrays: Implications for channel–lobe transition zones: Marine Geology, v. 381, p. 181–193.

Draganits, E., Schlaf, J., Grasemann, B., and Argles, T., 2008, Giant submarine landslide grooves in the Neoproterozoic / Lower Cambrian Phe Formation, Northwest Himalaya: Mechanisms of formation and palaeogeographic implications: Sedimentary Geology, v. 205, p. 126–141.

Dżułyński, S., 1965, New data on experimental production of sedimentary structures: Journal of Sedimentary Petrology, v. 35, p. 196–212.

Dżułyński, S., and Radomski, A., 1955, Origin of groove casts in the light of turbidity current hypothesis: Acta Geologica Polonica, v. 5, p. 47–56.

Dżułyński. S., and Sanders, J.E., 1962, Current marks on firm mud bottoms: Connecticut Academy of Arts and Sciences, Transactions, v. 42, p. 57–96.

Dżułyński, S., and Walton, E.K., 1965, Sedimentary Features of Flysch and Greywackes: Amsterdam, Elsevier, Developments in Sedimentology, v. 7, 274 p.

Dżułyński, S., Ksiazkiewicz, M., and Kuenen, Ph.H., 1959, Turbidites in flysch of the Polish Carpathian Mountains: Geological Society of America, Bulletin, v. 70, p. 1089–1118.

Enos, P., 1969, Anatomy of a flysch: Journal of Sedimentary Petrology, v. 39, p. 680–723.

Felix, M., and Peakall, J., 2006, Transformation of debris flows into turbidity currents: mechanisms inferred from laboratory experiments: Sedimentology, v. 53, p. 107–123.

Fonnesu, M., Haughton, P., Felletti, F., and McCaffrey, W., 2015, Short length-scale variability of hybrid event beds and its applied significance: Marine and Petroleum Geology, v. 67, p. 583–603.

Fonnesu, M., Patacci, M., Haughton, P.D.W., Felletti, F., and McCaffrey, W.D., 2016, Hybrid event beds generated by local substrate delamination on a confined-basin floor: Journal of Sedimentary Research, v. 86, p. 929–943.

Fonnesu, M., Felletti, F., Haughton, P.D.W., Patacci, M., and McCaffrey, W.D., 2018, Hybrid event bed character and distribution linked to turbidite system sub-environments: The North Appenine Gottero Sandstone (north-west Italy): Sedimentology, v. 65, p. 151–190.

Gladstone, C., McClelland, H.L.O., Woodcock, N.H., Pritchard, D., and Hunt, J.E., 2018, The formation of convolute lamination in mud-rich turbidites: Sedimentology, v. 65, p. 1800–1825.

Grundvåg, S.-A., Johannessen, E.P., Helland-Hansen, W., and Plink-Björklund, P., 2014, Depositional architecture and evolution of progradationally stacked lobe complexes in the Eocene Central Basin of Spitsbergen: Sedimentology, v. 61, p. 535–569.

Hall, J., 1843, Geology of New York, Part 4, Comprising the Survey of the Fourth Geological District: Albany, Charles Van Benthuyson and Sons, 683 p.

Hampton, M.A., 1970, Subaqueous Debris Flow and Generation of Turbidity Currents [Ph.D. Thesis]: Stanford University, California, 180 p.

Hansen, L.A.S., Hodgson, D.M., Pontén, A., Bell, D., and Flint, S., 2019, Quantification of basin-floor fan pinchouts: Examples from the Karoo Basin, South Africa: Frontiers in Earth Science, v. 7, doi:10.3389/feart.2019.00012.

Haughton, P.D., Barker, S.P., and McCaffrey, W.D., 2003, 'Linked' debrites in sand-rich turbidite systems–origin and significance: Sedimentology, v. 50, p. 459–482.

Haughton, P., Davis, C., McCaffrey, W., and Barker, S., 2009, Hybrid sediment gravity flow deposits classification, origin and significance: Marine and Petroleum Geology, v. 26, p. 1900–1918.

Heerema, C.J., Talling, P.J., Cartigny, M.J., Paull, C.K., Bailey, L., Simmons, S.M., Parsons, D.R., Clare, M.A., Gwiazda, R., Lundsten, E., Anderson, K., Maier, K.L., Xu, J.P., Sumner, E.J., Rosenberger, K., Gales, J., McGann, M., Carter, L., Pope, E., and Monterey Coordinated Canyon Experiment (CCE) Team, 2020, What determines the downstream evolution of turbidity currents?: Earth and Planetary Science Letters, v. 532, doi:10.1016/j.epsl.2019.116023.

Hermidas, N., Eggenhuisen, J.T., Jacinto, R.S., Luthi, S.M., Toth, F., and Pohl, F., 2018, A classification of clay-rich subaqueous density flow structures: Journal of Geophysical Research: Earth Surface, v. 123, p. 945–966.

Hodgson, D.M., 2009, Origin and distribution of bipartite beds in sand-rich submarine fans: constraints from the Tanqua depocentre, Karoo Basin, South Africa: Marine and Petroleum Geology, v. 26, p. 1940–1956.

Humair, F., Abellan, A., Carrea, D., Matasci, B., Epard, J.L., and Jaboyedoff, M., 2015, Geological layers detection and characterisation using high resolution 3D point clouds: Example of a box-fold in the Swiss Jura Mountains: European Journal of Remote Sensing. v. 48, p. 541–568.

Hussain, A., Haughton, P.D.W., Shannon, P.M., Turner, J.N., Pierce, C.S., Obradors-Latre, A., Barker, S.P., and Martinsen, O.J., 2020, High-resolution X-ray fluorescence profiling of hybrid event beds: Implications for sediment gravity flow behaviour and deposit structure: Sedimentology, v. 67, p. 2850-2882.

Kane, I.A., and Hodgson, D.M., 2011, Sedimentological criteria to differentiate submarine channel levee subenvironments: Exhumed examples from the Rosario Fm. (Upper Cretaceous) of Baja California, Mexico, and the Fort Brown Fm. (Permian), Karoo Basin, S. Africa: Marine and Petroleum Geology, v. 28, p. 807–823.

Kane, I.A., and Pontén, A.S.M., 2012, Submarine transitional flow deposits in the Paleogene Gulf of Mexico: Geology, v. 40, p. 1119–1122.

Kane, I.A., McCaffrey, W.D., and Peakall, J., 2010, On the origin of paleocurrent complexity within deep marine channel levees: Journal of Sedimentary Research, v. 80, p. 54–66.

Kane, I.A., Pontén, A.S.M., Vangdal, B., Eggenhuisen, J.T., Hodgson, D.M., and Spychala, Y.T., 2017, The stratigraphic record and processes of turbidity current transformation across deep-marine lobes: Sedimentology, v. 64, p. 1236–1273.

Kneller, B.C., and McCaffrey, W.D., 2003, The interpretation of vertical sequences in turbidite beds: The influence of longitudinal flow structure: Journal of Sedimentary Research, v. 73, p. 706–713.

Lowe, D.R., and Guy, M., 2000, Slurry-flow deposits in the Britannia Formation (Lower Cretaceous), North Sea: a new perspective on the turbidity current and debris flow problem: Sedimentology, v. 47, p. 31–70.

McClelland, H.L.O., Woodcock, N.H., and Gladstone, C., 2011, Eye and sheath folds in turbidite convolute lamination: Aberystwyth Grits Group, Wales: Journal of Structural Geology, v. 33, p. 1140–1147.

Middleton, G.V., and Hampton, M.A., 1973, Sediment gravity flows: mechanics of flow and deposition, *in* Middleton, G.V., and Bouma, A.H., eds., Turbidites and Deep-water Sedimenttion: SEPM Pacific Section short course, p. 1–38.

Middleton, G.V., and Hampton, M.A., 1976, Subaqueous sediment transport and deposition by sediment gravity flows, *in* Stanley, D.H., and Swift, D.J.P., eds., Marine Sediment Transport and Environmental Management: New York, John Wiley & Sons, p. 197–218.

Mohrig, D., Ellis, C., Parker, G., Whipple, K.X., and Hondzo, M., 1998, Hydroplaning of subaqueous debris flows. Geological Society of America, Bulletin, v. 110, p. 387–394.

Mueller, P., Patacci, M., and Di Giulio, A., 2021, Hybrid event distribution in a mixed siliciclastic–calcareous turbidite succession: a cross-current perspective from the Bordighera Sandstone, Ligurian Alps, NW Italy: Italian Journal of Geosciences, v. 140, p. 255-274.

Mutti, E., and Normark, W.R., 1987, Comparing examples of modern and ancient turbidite systems: Problems and concepts, *in* Legget, J.K., and Zuffa, G.G., eds., Marine Clastic Sedimentology: Concepts and Case Studies: Graham & Trotman, p. 1–38.

Navarro, L., and Arnott, R.W.C., 2020, Stratigraphic record in the transition from basin floor to continental slope sedimentation in the ancient passive-margin Windermere turbidite system: Sedimentology, v. 67, p. 1710–1749.

Necker, F., Härtel, C., Kleiser, L., and Meiburg, E., 2002, High-resolution simulations of particle-driven gravity currents: International Journal of Multiphase Flow, v. 28, p. 279–300.

Peakall, J., and Sumner, E.J., 2015, Submarine channel flow processes and deposits: A process–product perspective: Geomorphology, v. 244, p. 95–120.

Peakall, J., Best, J., Baas, J.H., Hodgson, D.M., Clare, M.A., Talling, P.J., Dorrell, R.M., and Lee, D.R., 2020, An integrated process-based model of flutes and tool marks in deep-water environments: Implications for palaeohydraulics, the Bouma sequence and hybrid event beds: Sedimentology, v. 67, p. 1601–1666.

Pett, J.W., and Walker, R.G., 1971, Relationship of flute cast morphology to internal sedimentary structures in turbidites: Journal of Sedimentary Petrology, v. 41, p. 114–128.

Pierce, C.S., Haughton, P.D.W., Shannon, P.M., Pulham, A.J., Barker, S.P., and Martinsen, O.J., 2018, Variable character and diverse origin of hybrid event beds in a sandy submarine fan system, Pennsylvanian Ross Sandstone Formation, western Ireland: Sedimentology, v. 65, p. 952–992.

Reineck, H.E., and Singh, I.B., 1973, Depositional Sedimentary Environments. Springer-Verlag, Berlin, Germany, 412 p.

Schmitz, B., Holst, C., Medic, T., Lichti, D.D., and Kuhlmann, H., 2019, How to efficiently determine the range precision of 3D terrestrial laser scanners: Sensors, v. 19, doi:10.3390/s19061466.

Schofield, D.I., Davies, J.R., Waters, R.A., Williams, M., and Wilson, D., 2008, A new Early Silurian turbidite system in Central Wales: insights into eustatic and tectonic controls on deposition in the southern Welsh Basin: Geological Magazine, v. 146, p. 121–132.

Sequeiros, O.E., Naruse, H., Endo, N., Garcia, M.H., and Parker, G., 2009, Experimental study on self-accelerating turbidity currents: Journal of Geophysical Research, Oceans, v. 114, doi:10.1029/2008JC005149.

Sequeiros, O.E., Mosquera, R., and Pedocchi, F., 2018, Internal structure of a self-accelerating turbidity current: Journal of Geophysical Research, Oceans, v. 123, p. 6260–6276.

Shan, X., Shi, X., Clift, P.D., Qiao, S., Jin, L., Liu, J., Fang, X., Xu, T., Li, S., Kandasamy, S., Zhao, M., Zhu, Y., Zhang, H., Zhang, D., Wang, H., Li, Y., Yao, Z., Wang, S., and Xu, J., 2019a, Carbon isotope and rare earth element composition of Late Quaternary sediment gravity flow deposits on the mid shelf of East China Sea: Implications for provenance and origin of hybrid event beds: Sedimentology, v. 66, p. 1861–1895.

Shan, X., Shi, X., Qiao, S., Jin, L., Otharán, G.N.A., Zavala, C., Liu, J., Zhang, Y., Zhang, D., Xu, T., and Fu, C., 2019b, The fluid mud flow deposits represent mud caps of Holocene hybrid event beds from the widest and gentlest shelf: Marine Geology, v. 415, doi:10.1016/j.margeo.2019.06.004.

Smith, R., 2004, Turbidite systems influenced by structurally induced topography in the multi-sourced Welsh Basin: *in* Lomas, S.A., and Joseph, P., eds., Confined Turbidite Systems: Geological Society of London, Special Publication 222, p. 209–228.

Spychala, Y.T., Hodgson, D.M., and Lee, D.R., 2017a, Autogenic controls on hybrid bed distribution in submarine lobe complexes: Marine and Petroleum Geology, v. 88, p. 1078–1093.

Spychala, Y.T., Hodgson, D.M., Prélat, A., Kane, I.A., Flint, S.S., and Mountney, N.P., 2017b, Frontal and lateral submarine lobe fringes: Comparing sedimentary facies, architecture and flow processes: Journal of Sedimentary Research, v. 87, p. 75–96.

Stevenson, C.J., Peakall, J., Hodgson, D.M., Bell, D., and Privat, A., 2020, T_b or not T_b: Banding in turbidite sandstones: Journal of Sedimentary Research, v. 90, p. 821–842.

Talling, P.J., 2013, Hybrid submarine flows comprising turbidity current and cohesive debris flow: Deposits, theoretical and experimental analyses, and generalized models: Geosphere, v. 9, p. 460–488.

Talling P.J., Peakall, J., Sparks, R.S.J., Ócofaigh, C.S., Dowdeswell, J.A., Felix, M., Wynn, R.B., Baas, J.H., Hogg, A.J., Masson, D.G., Taylor, J., and Weaver, P.P.E., 2002. Experimental constraints on shear mixing rates and processes: implications for the dilution of submarine debris flows. *In* Dowdeswell, J.A., and ÓCofaigh, C.S., Glacier-influenced Sedimentation on High-Latitude Continental Margins: Geological Society of London, Special Publication 203, p. 89–103.

Talling, P.J., Amy, L.A., Wynn, R.B., Peakall, J., and Robinson, M., 2004, Beds comprising debrite sandwiched within co-genetic turbidite: origin and widespread occurrence in distal depositional environments: Sedimentology, v. 51, p. 163–194.

Terlaky, V., and Arnott, R.W.C., 2014, Matrix-rich and associated matrix-poor sandstones: Avulsion splays in slope and basin-floor strata: Sedimentology, v. 61, p. 1175–1197.

Wang, Z., and Plate, E.C.H.J., 1996, A preliminary study on the turbulence structure of flows of non-Newtonian fluid: Journal of Hydraulic Research, v. 34, p. 345–361.

Wang, Z., Xu, J., Talling, P.J., Cartigny, M.J.B., Simmons, S.M., Gwiazda, R., Paull, C.K., Maier, K.L. and Parsons, D.R. (2020) Direct evidence of a high-concentration basal layer in a submarine turbidity current: Deep Sea Research Part I, v. 161, doi:10.1016/j.dsr.2020.103300.

Wilson, D., Davies, J.R., Waters, R.A., and Zalasiewiczt, J.A., 1992, A fault-controlled depositional model for the Aberystwyth Grits turbidite system: Geological Magazine, v. 129, p. 595–607.

Wood, A., and Smith, A.J., 1958, The sedimentation and sedimentary history of the Aberystwyth Grits (Upper Llandoverian): Geological Society of London, Quarterly Journal, v. 114, p. 163–195.

Zervas, D., Nichols, G.J., Hall, R., Smyth, H.R., Lüthje, C., and Murtagh, F., 2009, SedLog: A shareware program for drawing graphic logs and log data manipulation. Computers & Geosciences, v. 35, p. 2151–2159.

FIGURE CAPTIONS

Table 1.**—**Comparison of diagnostic properties of depositional environments in previous work and in the present study.

Table 2.**—**Overview of sole-mark data. Sole marks in bold refer to youngest type in beds with clearly crosscutting sole marks.

Fig. 1.**—**Theoretical model linking types of sole structure to type of sediment gravity flow and downslope distance (modified after Peakall et al. 2020). Here, the flow transforms downslope from turbulent flow via transitional flow to cohesive flow. If the flow transformation is reversed from cohesive to turbulent flow, the sequence of sole marks is also reversed. TF = turbulent flow; TETF = turbulence-enhanced transitional flow; LTPF = lower transitional plug flow; UTPF = upper transitional plug flow; QLPF = quasi-laminar plug flow; LPF = laminar plug flow.

Fig. 2.**—A**) Schematic diagram of an ideal flute mark (modified after Peakall et al. 2020) and example of flute marks below Bed 4a (Unit 4). **B**) Groove marks below Bed 7d (Unit 7). **C**) Schematic drawings of a fully formed chevron mark (planform on the left, and crosssection on the right, with arrow

denoting flow direction (modified after Allen, 1984) and example of a chevron mark below Bed 5d (Unit 5). **D**) Groove marks (gm) and a prominent tumble mark (tm) below Bed 5e (Unit 5).

Fig. 3.—Schematic diagram of various discontinuous tool marks (modified after Peakall et al. 2020). Black arrows denote motion of center of tool. Dashed arrows denote motion of point on surface of tool.

Fig. 4.—Schematic models of turbulent, transitional, and quasi-laminar flow types that sediment gravity flows can exhibit (modified after Baas et al. 2011). vsl = viscous sublayer.

Fig. 5.—Schematic geological reconstruction of the elongate basin in which the Aberystwyth Grits turbidite system was formed (after Cherns et al. 2006). The red dot shows the approximate position of the study area.

Fig. 6.—Site map of the fieldwork conducted NE of Aberarth. Black numbers next to log locations refer to Figures 10–12. Blue numbers denote 3D laser scanning sites 1 and 2. Northings and Eastings are based on Universal Transverse Mercator coordinates.

Fig. 7.—Southwestern part of the composite drone image of the coastal outcrop between Aberarth and Llannon. **A**) Original image. **B**) Interpreted image with lithological units and bed correlations.

Fig. 8.—Central part of the composite drone image of the coastal outcrop between Aberarth and Llannon. **A**) Original image. **B**) Interpreted image with lithological units and bed correlations.

Fig. 9.—Northeastern part of the composite drone image of the coastal outcrop between Aberarth and Llannon. **A**) Original image. **B**) Interpreted image with lithological units and bed correlations.

Fig. 10.—Drawings and photographs of sedimentary logs in: **A**) Unit 1, **B**) Unit 3, and **C**) Unit 7, interpreted as channel–lobe transition zone. Beds 1a-e, 3a-d, and 7a-e contain sole marks. **D**) key to

textural and structural features in logs. See Table 2 for observed sole-mark types below event beds 1a-d, 3a-d, and 7a-e.

Fig. 11.**—**Drawings and photographs of sedimentary logs in: **A**) Unit 2, and **B**) Unit 4, interpreted as levee and channel-fill, respectively. Beds 2a-f and 4a-c contain sole marks. See Fig. 10D for key to textural and structural features in logs. See Table 2 for observed sole-mark types below event beds 2a-f and 4a-c.

Fig. 12.**—**Drawings and photographs of sedimentary logs in: (**A**) Unit 5, and (**B**) Unit 6, interpreted as lobe fringe and lobe axis (or off-axis), respectively. Beds 5a-e and 6a-e contain sole marks (Table 2). See Fig. 10D for key to textural and structural features in logs. LR = large ripples, and LABW = large-amplitude bed waves (*sensu* Baas et al. 2016a). See Table 2 for observed sole-mark types below event beds 5a-e and 6a-e.

Fig. 13.**—**Equal-area circular diagram with paleoflow-direction data from the study area, based on flute marks, discontinuous tool marks, and continuous tool marks. Number in center is total number of measurements, n. Yellow sectors show frequency percentages for a class width of 10°. Pink sector denotes mean vector azimuth (red bisectorial line) and length (sector length) and angular confidence interval (sector width) for the mean vector for a significance interval, a, of 5% (Baas 2000). Blue arrows give mean vector azimuths for the various depositional environments. Long continuous and short dashed blue lines distinguish statistically significant means from insignificant means, because of small n value, at a = 5%. CLTZ = channel–lobe transition zone.

Fig. 14.**—**Transitional-flow deposit with low-amplitude bed waves in Unit 6. The bedforms are c. 10–20 mm high and c. 400–450 mm long. Flow direction was from right to left.

Fig. 15.**—**Examples of sole-mark types. **A**) Large groove mark below Bed 7a, 0.25 m wide. **B**) Skim marks below Bed 5c, up to 15 mm in width. **C**) Predominantly spindle flute marks below Bed 2c. Grain-

size scale is 110 mm long. **D**) Parabolic flute marks below Bed 5b. The flute marks in the center of the bed are c. 70 mm long. Also shown is Bed 5a with a prominent groove mark, c. 50 mm wide.

Fig. 16.—**A**) Frequency distributions of main sole-mark types in debrites, hybrid event beds, and turbidites, with examples of event beds and youngest sole marks (from left to right: groove marks below Beds 3b and 6b; parabolic flute marks below Bed 4c). The grooves below Bed 6b are c. 10 mm wide. The flutes are c. 50 mm long and wide. **B**) Frequency distributions of main sole-mark types in divisions of event beds immediately above the sole-mark surface. n = number of data; ppl = plane-parallel-laminated division; rxl = ripple-cross-laminated division. All pie charts are based on the youngest sole marks below each bed.

Fig. 17.—Sole-mark type (n = 67) and type of sediment-gravity-flow deposit (n = 124) as a function of depositional environment in the study area. Also shown are dominant lower divisions in beds with sole marks. Subordinate lower divisions are between brackets. M = massive division; ppl = plane-parallel-laminated division; B = banded division; D = debritic division. CLTZ = channel–lobe transition zone.

Fig. 18.—**A**) Mean length and depth of flute marks, and **B**) mean width and depth of groove marks, in various depositional environments in the study area. Dark blue and green lines denote longitudinal trends. Dashed, blue and green lines signify transverse trends. No depths of flutes are available for the lobe-axis environment.

Fig. 19.—Schematic downstream-evolution paths of principal flows in the study area, based on the balance between turbulent forces and cohesive forces, represented by flow velocity and suspended clay concentration, respectively. **A**) Bypassing head of highly erosive hybrid flows. **B**) Body of the same hybrid flows. **C**) Transitional flows. **D**) Turbidity currents. CLTZ = channel–lobe transition zone. H1–H3 = hybrid-event-bed divisions of Haughton et al. (2003, 2009). Flutes were not found below the base of

transitional flow deposits (**C**), but these scour marks, possibly in combination with discontinuous tool marks, might appear in other sedimentary successions.

Fig. 20.—Schematic model for hybrid-event mechanics in the study area. Erosion of mud clasts from the bed occurs at the head of the flow, and the front of the flow transforms into a debris flow as the flow decelerates. Clasts at the base of this debris flow are dragged through the substrate, producing groove marks. Development of the hybrid event bed subsequently takes place via a combination of two processes: longitudinal segregation of clasts as bedload and vertical segregation of suspended load as a result of deceleration. This temporal deceleration progressively leads at a given point to more cohesive flows (H1, H2, H3a) and eventual formation of a true debris flow (H3b division). H1–H5 divisions *sensu* Haughton et al. (2009), H3a and H3b subdivisions *sensu* Hussain et al. (2020). See text for further details.

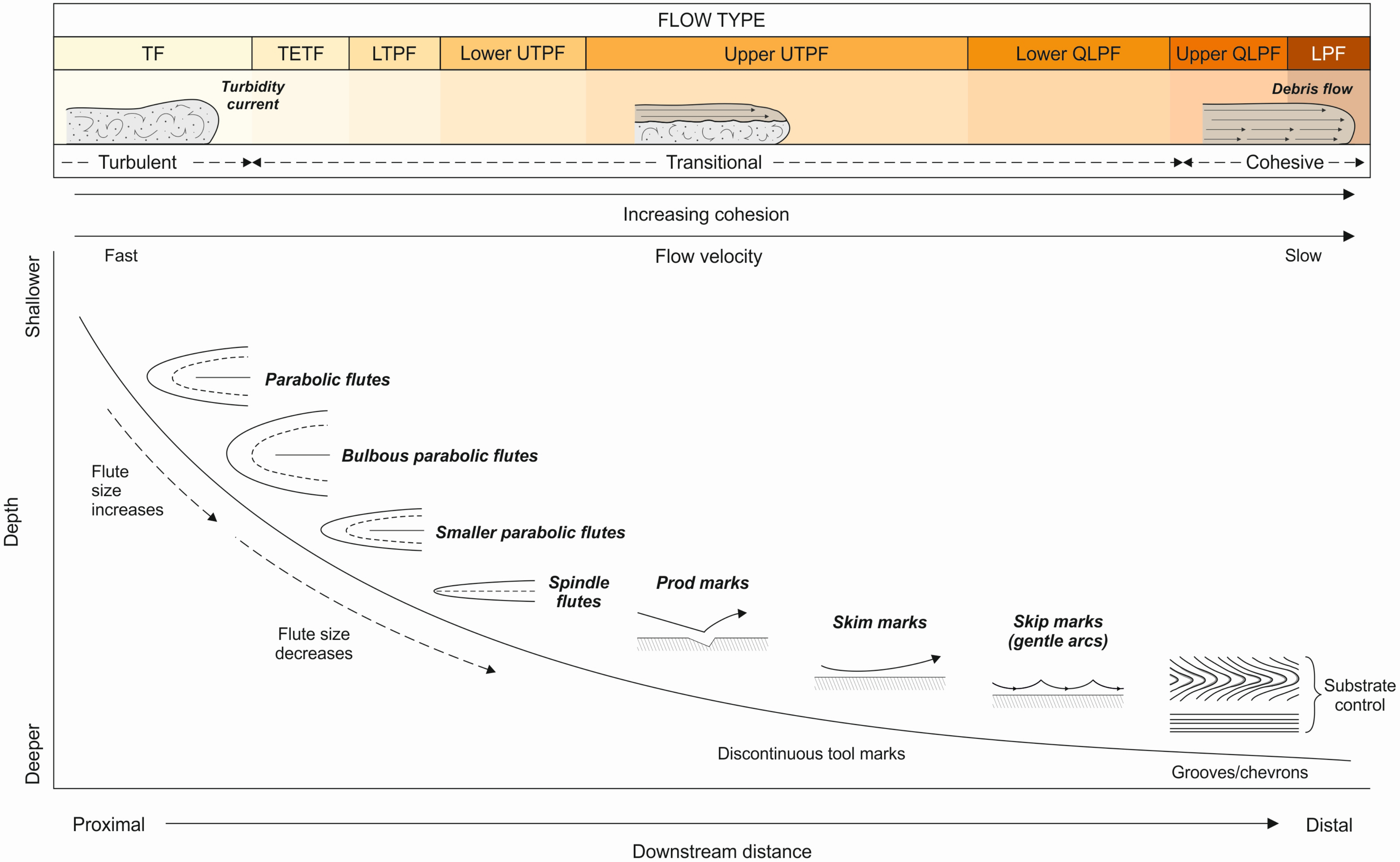
FLOW TYPE
TF
TETF
LTPF
Lower UTPF
Upper UTPF
Lower QLPF
Upper QLPF
LPF
Turbidity current
Debris flow
Turbulent
Transitional
Cohesive
Increasing cohesion
Fast
Flow velocity
Slow
Shallower
Depth
Deeper
Parabolic flutes
Bulbous parabolic flutes
Smaller parabolic flutes
Spindle flutes
Prod marks
Skim marks
Skip marks (gentle arcs)
Substrate control
Flute size increases
Flute size decreases
Discontinuous tool marks
Grooves/chevrons
Proximal
Distal
Downstream distance

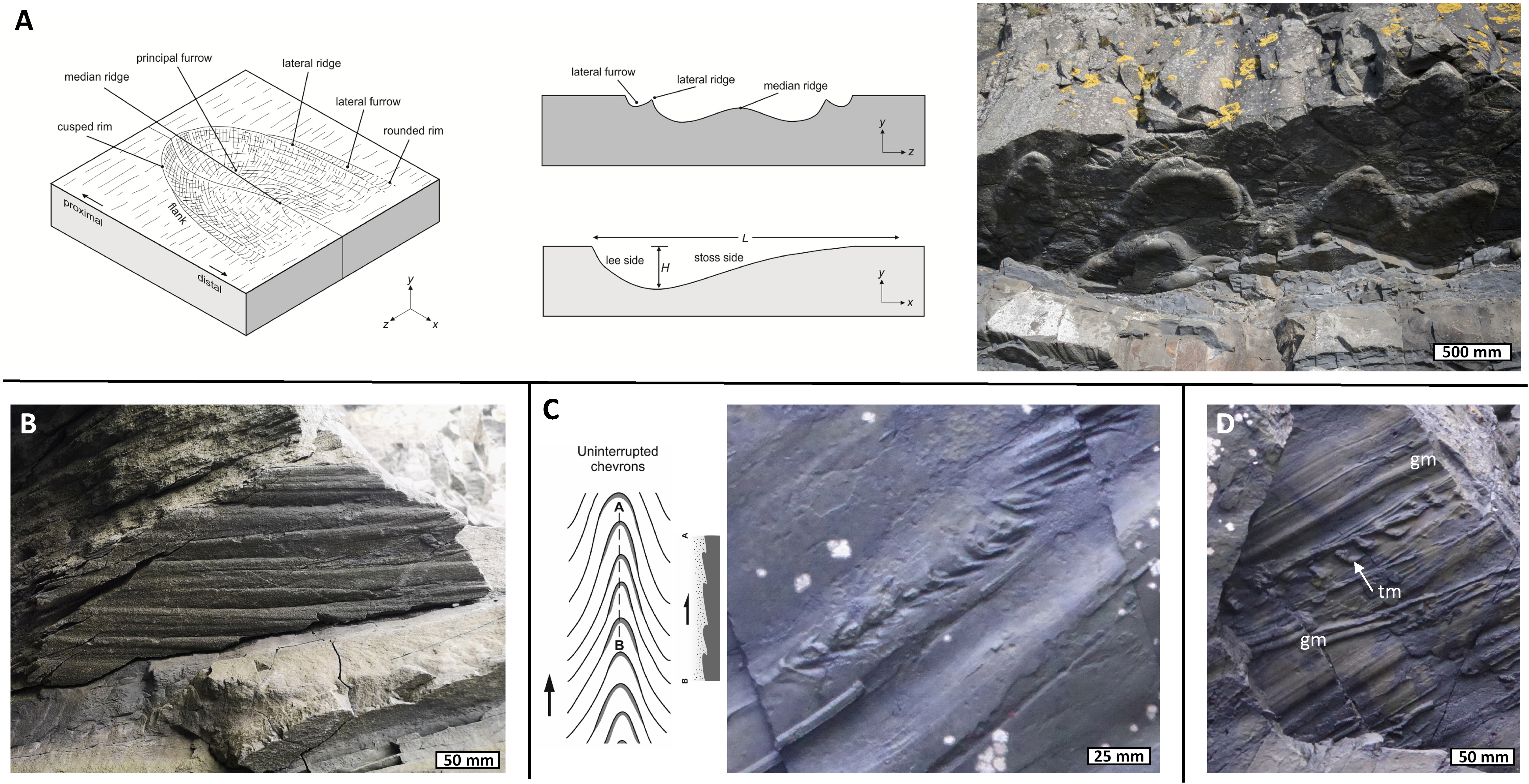
A
principal furrow
lateral ridge
median ridge
lateral furrow
cusped rim
rounded rim
proximal
flank
distal
y
z
x
lateral furrow
lateral ridge
median ridge
L
lee side
H
stoss side
500 mm
B
50 mm
C
Uninterrupted chevrons
A
B
25 mm
D
gm
tm
gm
50 mm

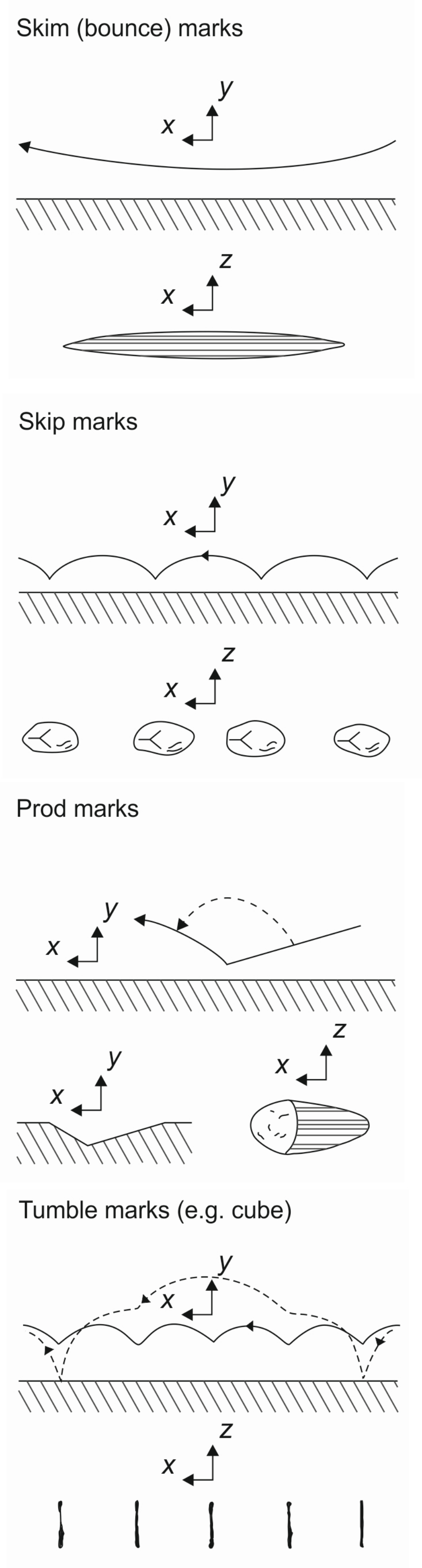
Skim (bounce) marks
y
x
z
x
Skip marks
y
x
z
x
Prod marks
y
x
y
x
z
x
Tumble marks (e.g. cube)
y
x
z
x

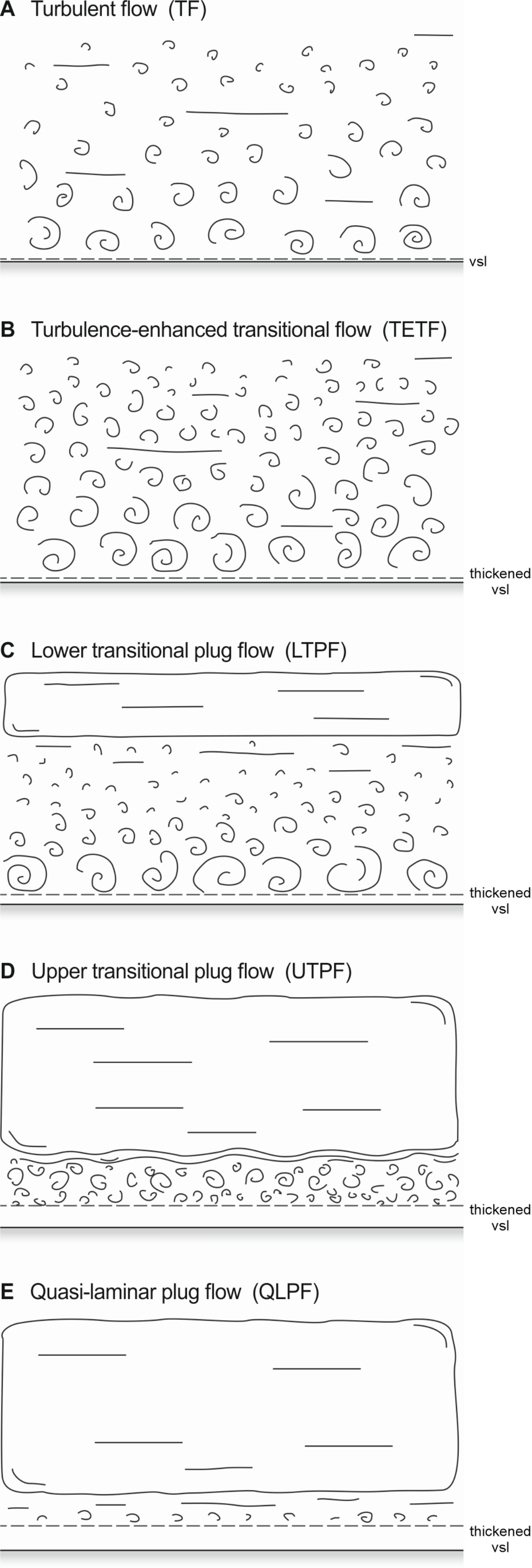
A Turbulent flow (TF)
vsl
B Turbulence-enhanced transitional flow (TETF)
thickened vsl
C Lower transitional plug flow (LTPF)
thickened vsl
D Upper transitional plug flow (UTPF)
thickened vsl
E Quasi-laminar plug flow (QLPF)
thickened vsl

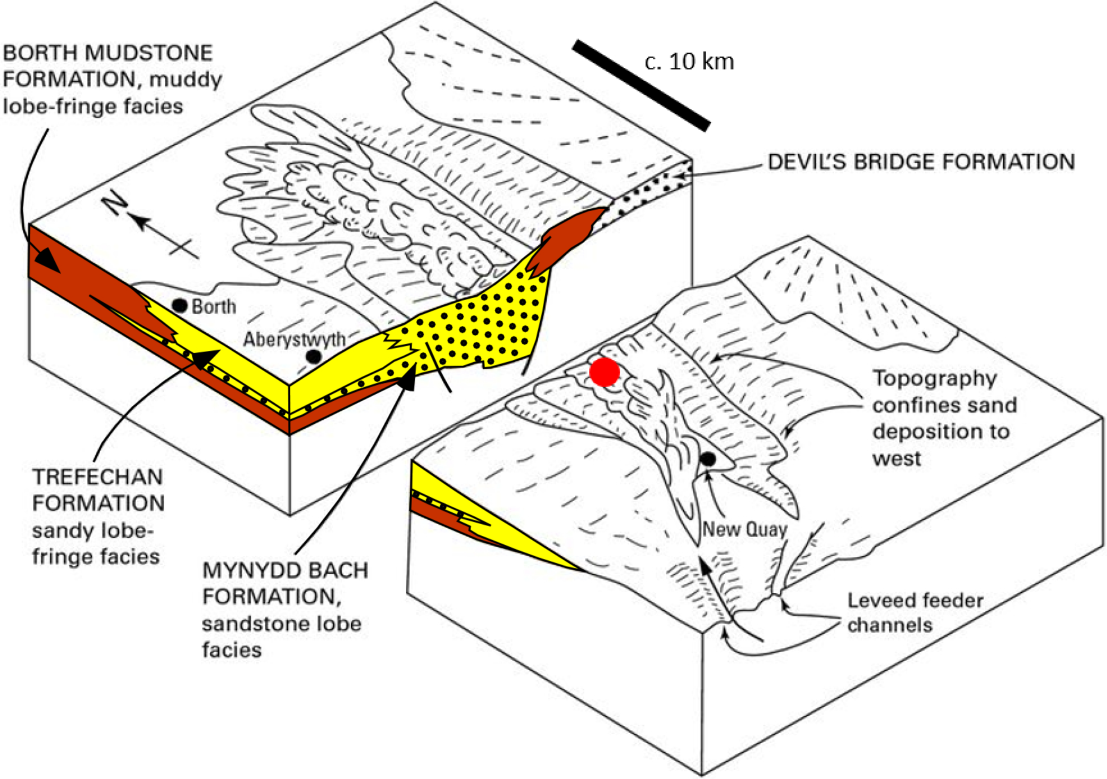
BORTH MUDSTONE FORMATION, muddy lobe-fringe facies
c. 10 km
DEVIL'S BRIDGE FORMATION
N
Borth
Aberystwyth
Topography confines sand deposition to west
TREFECHAN FORMATION sandy lobe-fringe facies
New Quay
MYNYDD BACH FORMATION, sandstone lobe facies
Leveed feeder channels

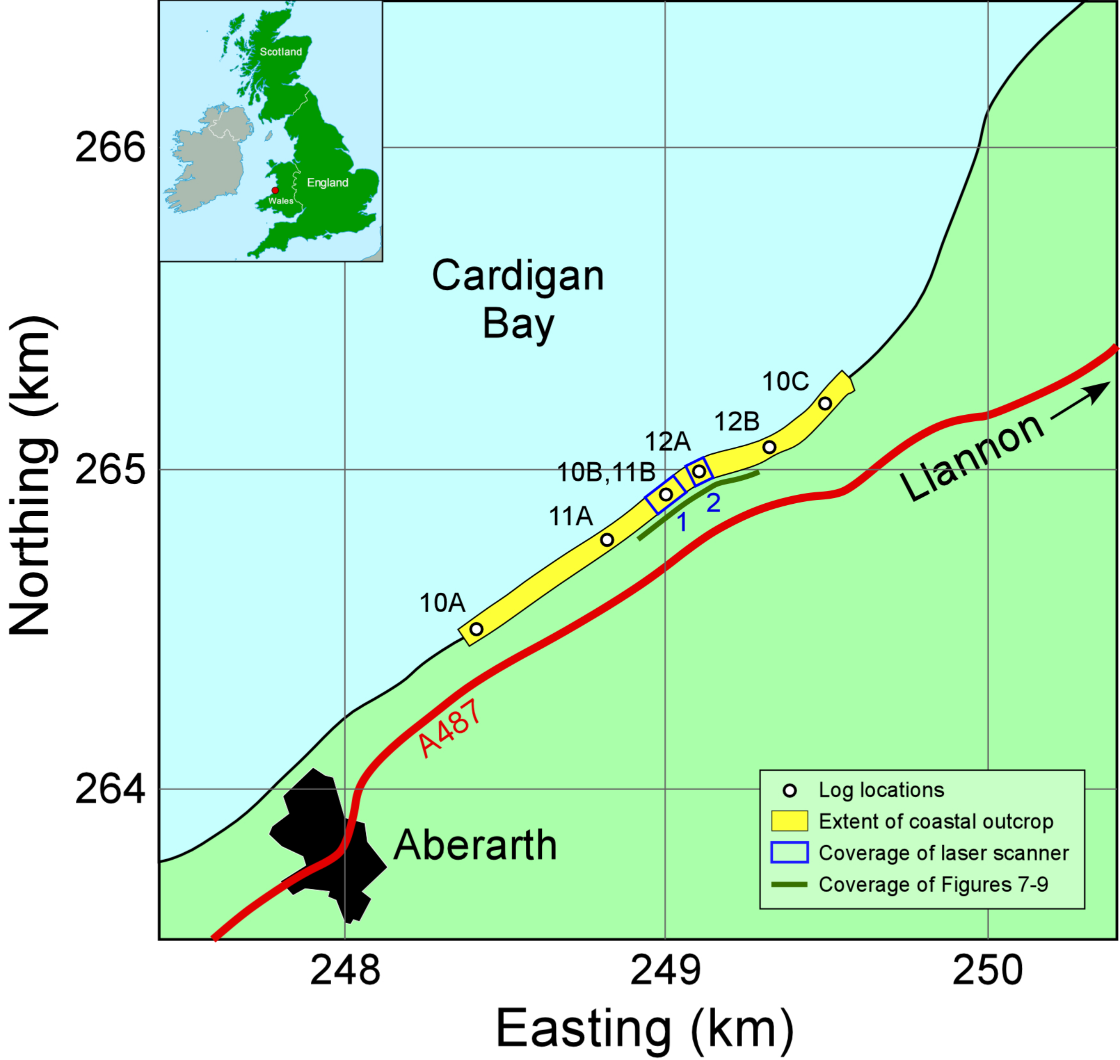
Scotland
England
Wales
Cardigan
Bay
10C
12B
12A
10B,11B
11A
10A
1
2
Llannon
A487
Aberarth
Log locations
Extent of coastal outcrop
Coverage of laser scanner
Coverage of Figures 7-9
266
265
264
248
249
250
Northing (km)
Easting (km)

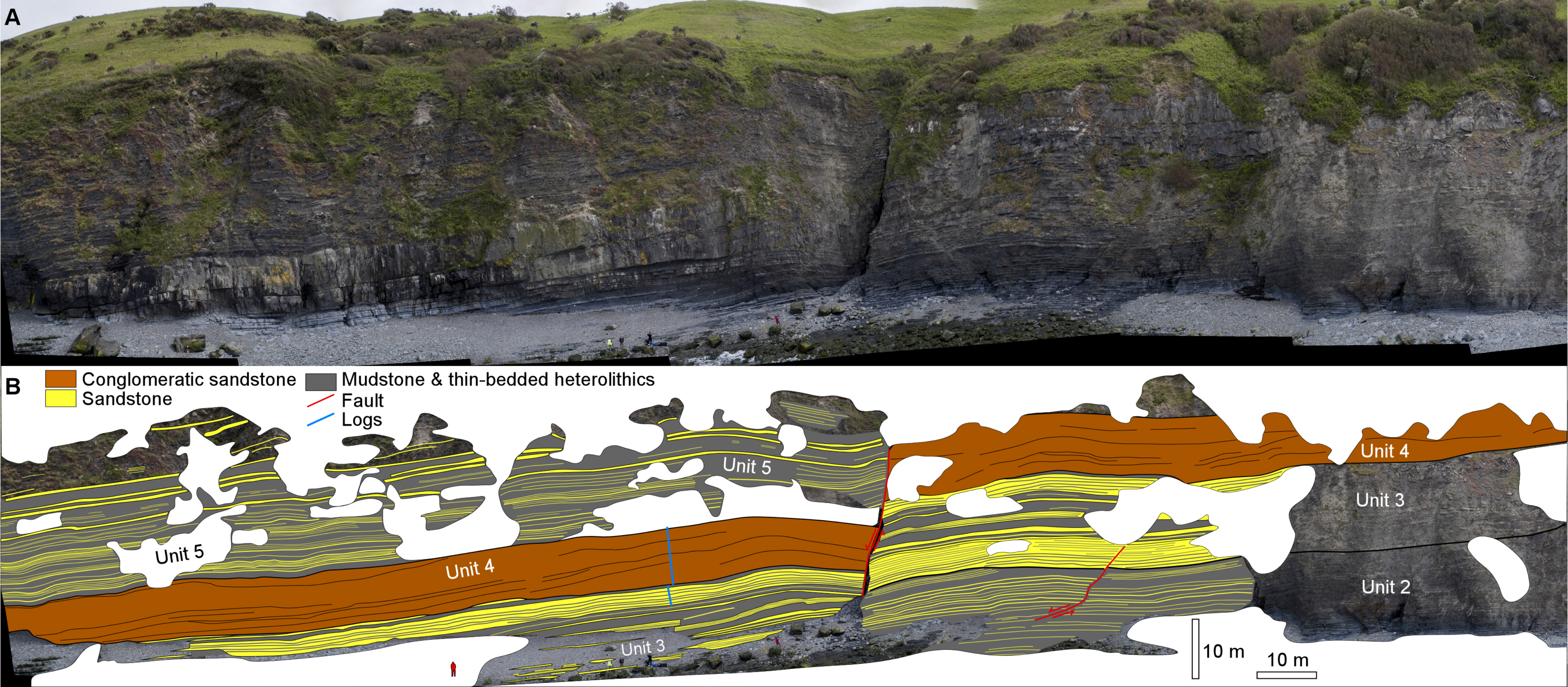
A
B
Conglomeratic sandstone
Sandstone
Mudstone & thin-bedded heterolithics
Fault
Logs
Unit 5
Unit 5
Unit 4
Unit 4
Unit 3
Unit 3
Unit 2
10 m
10 m

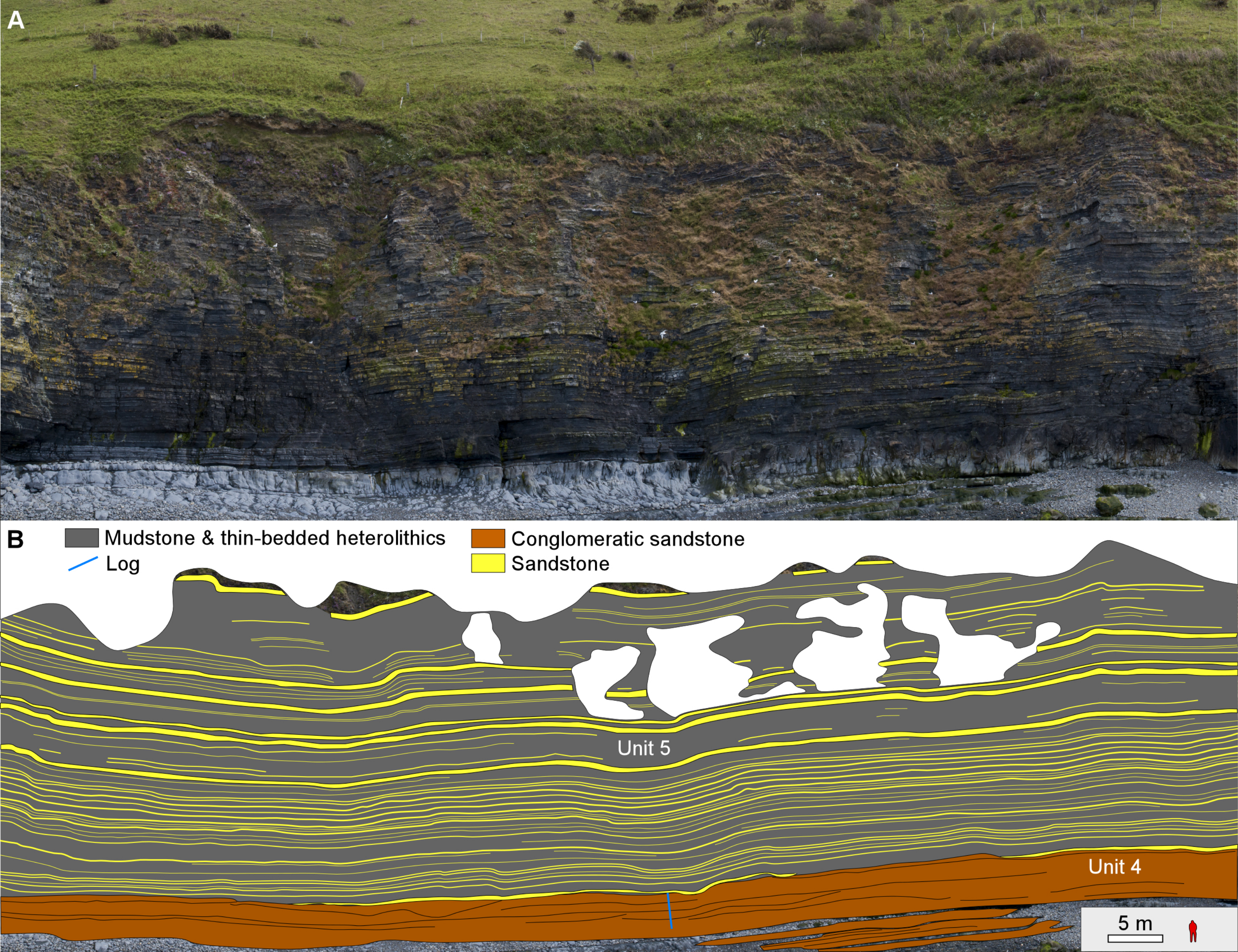
A
B
Mudstone & thin-bedded heterolithics
Log
Conglomeratic sandstone
Sandstone
Unit 5
Unit 4
5 m

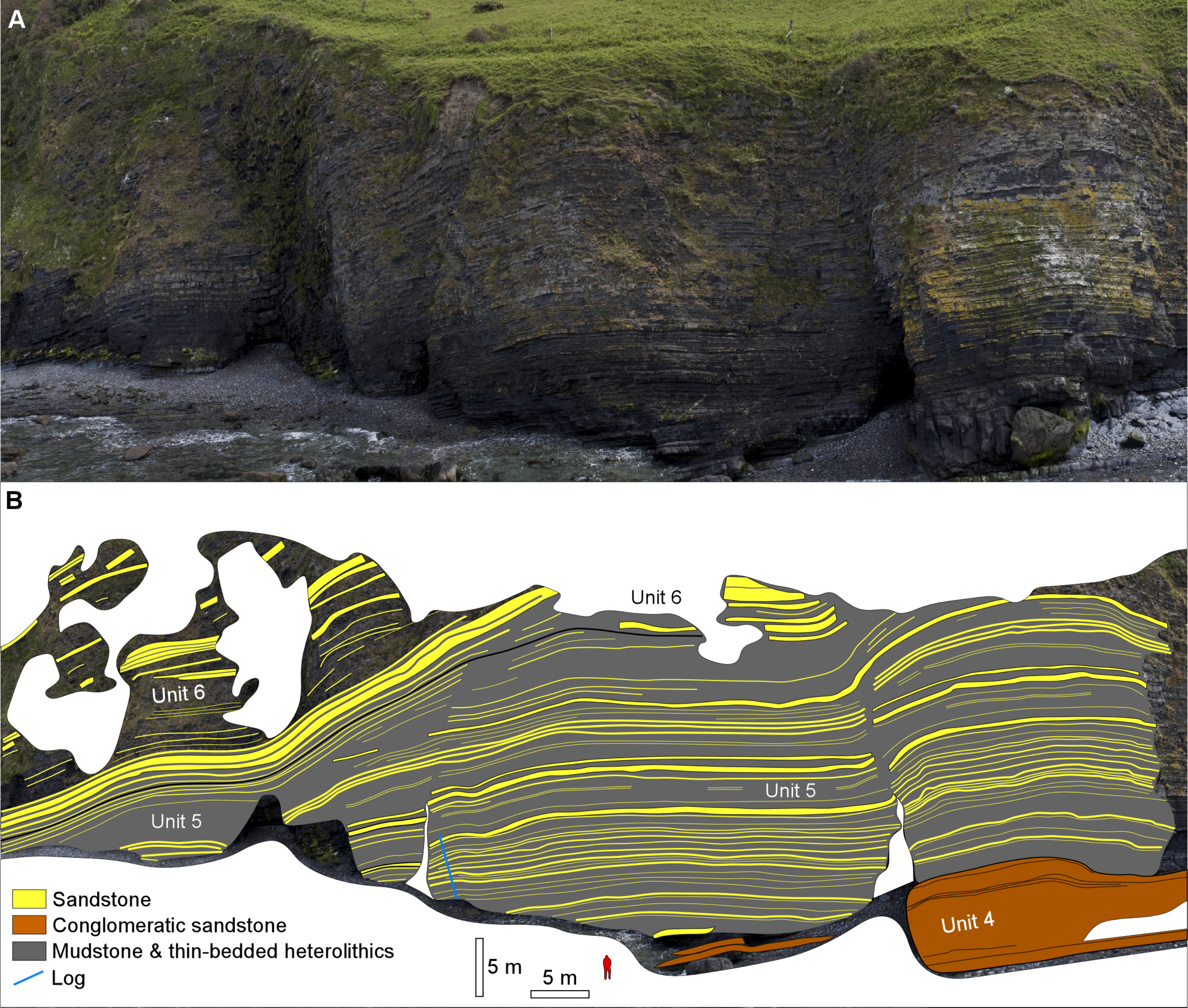
A
B
Unit 6
Unit 6
Unit 5
Unit 5
Unit 4
Sandstone
Conglomeratic sandstone
Mudstone & thin-bedded heterolithics
Log
5 m
5 m

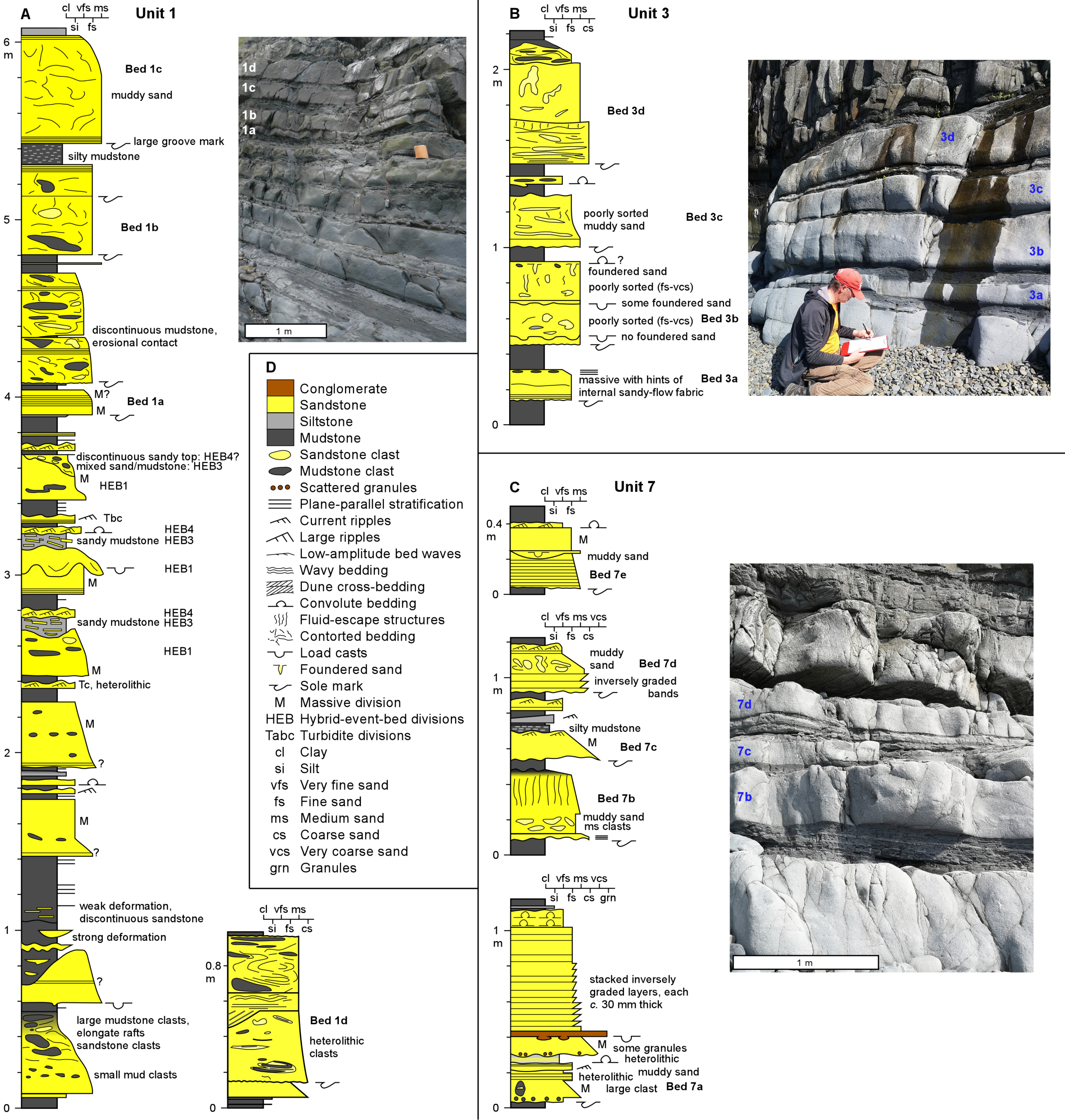

A
Unit 1
cl vfs ms
si fs
6 m
5
4
3
2
1
0
Bed 1c
muddy sand
large groove mark
silty mudstone
Bed 1b
discontinuous mudstone, erosional contact
M?
Bed 1a
M
discontinuous sandy top: HEB4?
mixed sand/mudstone: HEB3
M
HEB1
Tbc
HEB4
sandy mudstone HEB3
HEB1
M
HEB4
sandy mudstone HEB3
HEB1
M
Tc, heterolithic
M
?
M
?
weak deformation, discontinuous sandstone
strong deformation
?
large mudstone clasts, elongate rafts sandstone clasts
small mud clasts
1d
1c
1b
1a
1 m
cl vfs ms
si fs cs
0.8 m
0
Bed 1d
heterolithic clasts
D
Conglomerate
Sandstone
Siltstone
Mudstone
Sandstone clast
Mudstone clast
Scattered granules
Plane-parallel stratification
Current ripples
Large ripples
Low-amplitude bed waves
Wavy bedding
Dune cross-bedding
Convolute bedding
Fluid-escape structures
Contorted bedding
Load casts
Foundered sand
Sole mark
M Massive division
HEB Hybrid-event-bed divisions
Tabc Turbidite divisions
cl Clay
si Silt
vfs Very fine sand
fs Fine sand
ms Medium sand
cs Coarse sand
vcs Very coarse sand
grn Granules
B
Unit 3
cl vfs ms
si fs cs
2 m
1
0
Bed 3d
poorly sorted muddy sand
Bed 3c
?
foundered sand
poorly sorted (fs-vcs)
some foundered sand
poorly sorted (fs-vcs)
Bed 3b
no foundered sand
massive with hints of internal sandy-flow fabric
Bed 3a
3d
3c
3b
3a
C
Unit 7
cl vfs ms
si fs
0.4 m
0
M
muddy sand
Bed 7e
cl vfs ms vcs
si fs cs
1 m
0
muddy sand
Bed 7d
inversely graded bands
silty mudstone
M
Bed 7c
Bed 7b
muddy sand ms clasts
7d
7c
7b
1 m
cl vfs ms vcs
si fs cs grn
1 m
0
stacked inversely graded layers, each c. 30 mm thick
M
some granules
heterolithic
heterolithic
muddy sand
M
large clast
Bed 7a

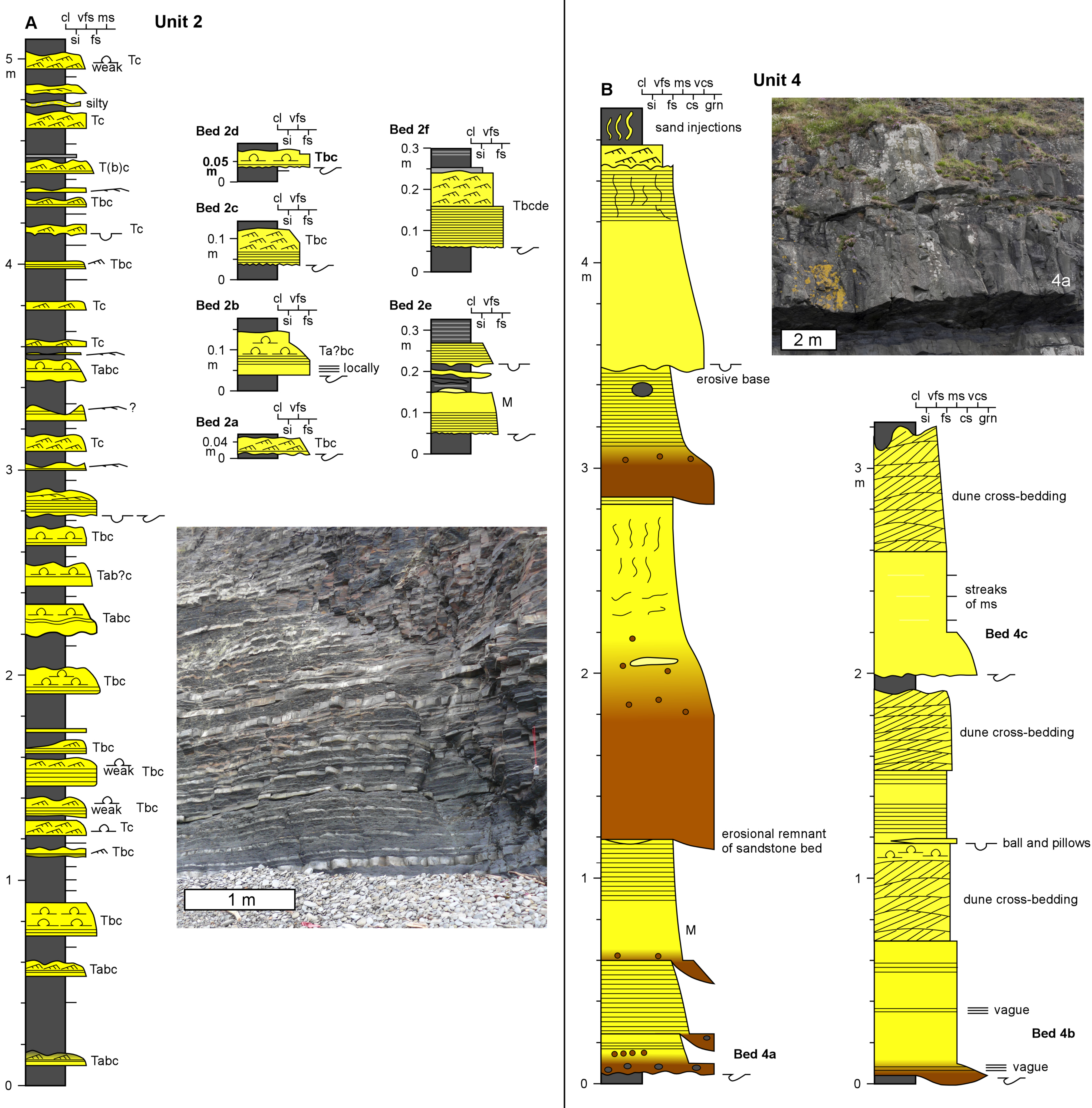

A
Unit 2
cl vfs ms
si fs
5 m
weak
Tc
silty
Tc
T(b)c
Tbc
Tc
4
Tbc
Tc
Tc
Tabc
?
Tc
3
Tbc
Tab?c
Tabc
2
Tbc
Tbc
weak
Tbc
weak
Tbc
Tc
Tbc
1
Tbc
Tabc
Tabc
0
Bed 2d
0.05 m
0
Tbc
Bed 2c
0.1 m
0
Tbc
Bed 2b
0.1 m
0
Ta?bc
locally
Bed 2a
0.04 m
0
Tbc
Bed 2f
0.3 m
0.2
0.1
0
Tbcde
Bed 2e
0.3 m
0.2
0.1
0
M
1 m
B
Unit 4
cl vfs ms vcs
si fs cs grn
sand injections
4 m
erosive base
3
2
erosional remnant
of sandstone bed
1
M
Bed 4a
0
2 m
4a
3 m
dune cross-bedding
streaks
of ms
Bed 4c
2
dune cross-bedding
ball and pillows
1
dune cross-bedding
vague
Bed 4b
vague
0

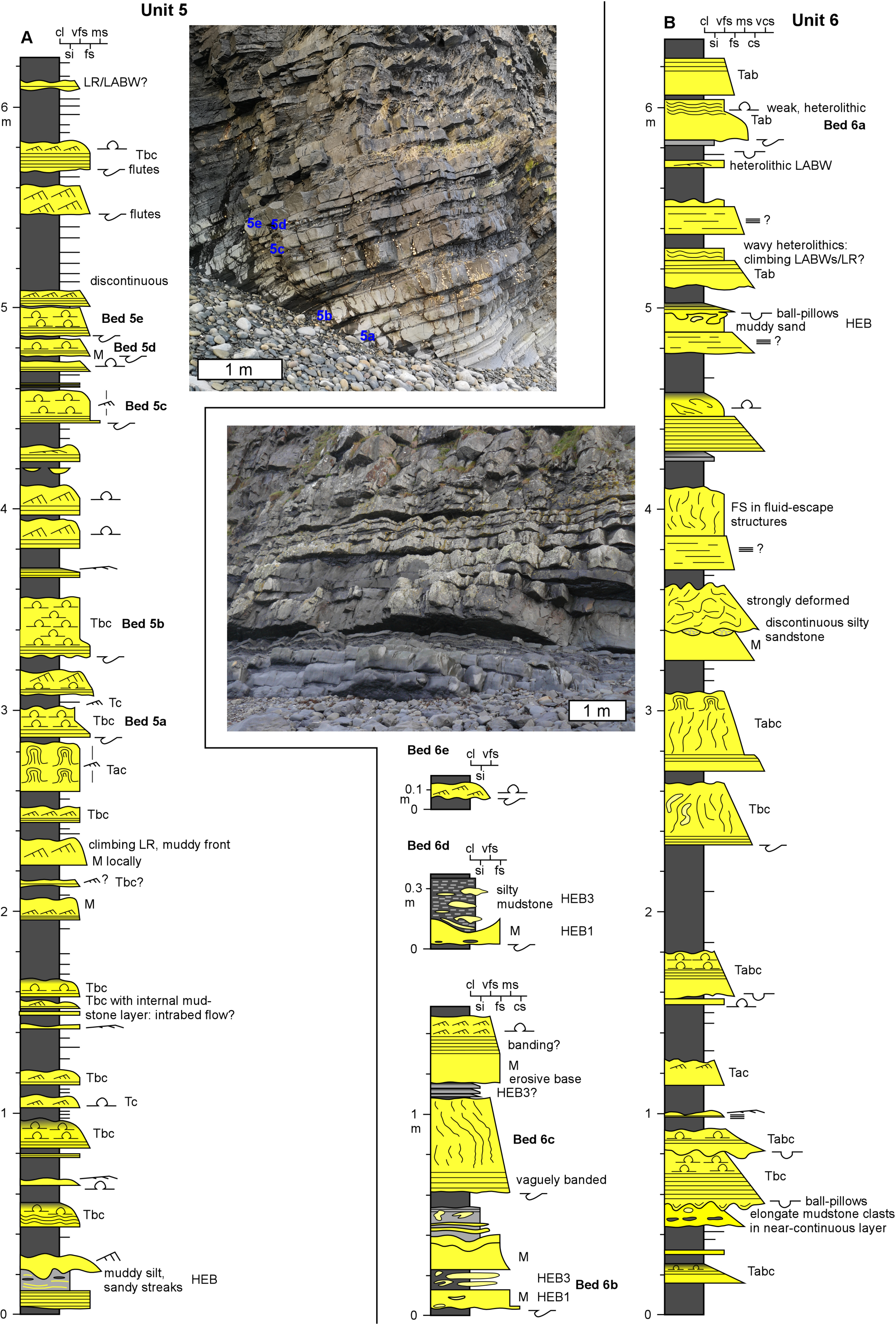

Unit 5
A
cl vfs ms
si fs
LR/LABW?
6
m
Tbc
flutes
flutes
discontinuous
5
Bed 5e
Bed 5d
M
Bed 5c
4
Tbc
Bed 5b
Tc
3
Tbc
Bed 5a
Tac
Tbc
climbing LR, muddy front
M locally
? Tbc?
2
M
Tbc
Tbc with internal mud-
stone layer: intrabed flow?
Tbc
Tc
1
Tbc
Tbc
muddy silt,
sandy streaks
HEB
0
5e
5d
5c
5b
5a
1 m
1 m
Bed 6e
cl vfs
si
0.1
m
0
Bed 6d
cl vfs
si fs
0.3
m
silty
mudstone
HEB3
M
HEB1
0
cl vfs ms
si fs cs
banding?
M
erosive base
HEB3?
1
m
Bed 6c
vaguely banded
M
HEB3
Bed 6b
M HEB1
0
B
cl vfs ms vcs
si fs cs
Unit 6
Tab
6
m
weak, heterolithic
Tab
Bed 6a
heterolithic LABW
?
wavy heterolithics:
climbing LABWs/LR?
Tab
5
ball-pillows
muddy sand
HEB
?
4
FS in fluid-escape
structures
?
strongly deformed
discontinuous silty
sandstone
M
3
Tabc
Tbc
2
Tabc
Tac
1
Tabc
Tbc
ball-pillows
elongate mudstone clasts
in near-continuous layer
Tabc
0

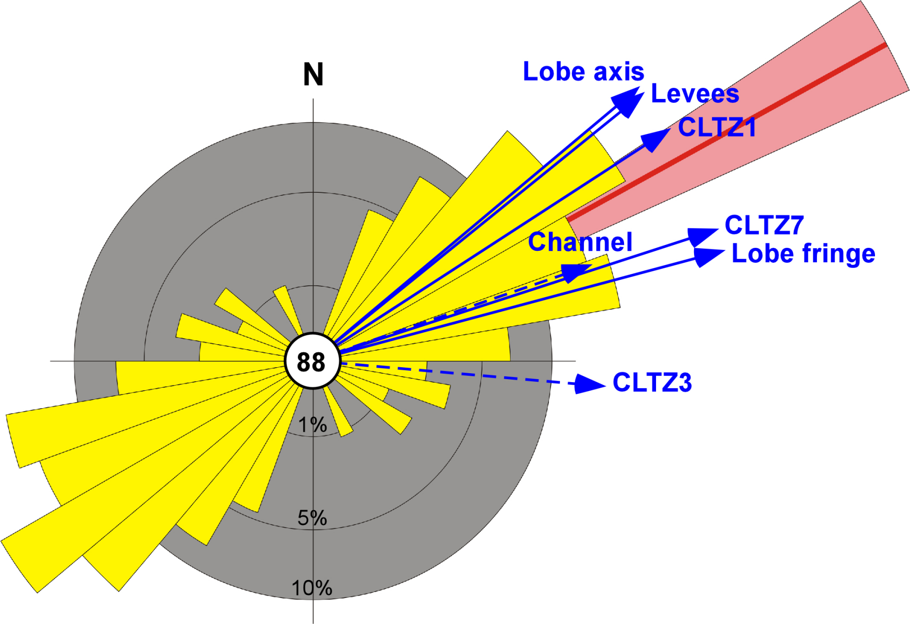
N
Lobe axis
Levees
CLTZ1
CLTZ7
Channel
Lobe fringe
88
CLTZ3
1%
5%
10%


100 mm

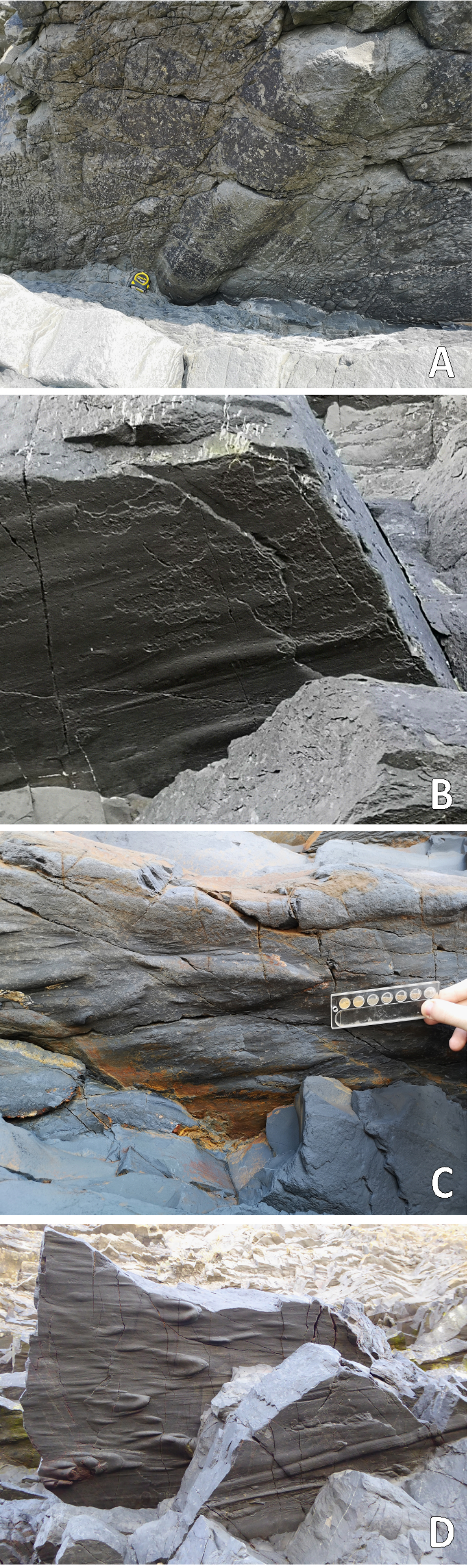
A
B
C
D

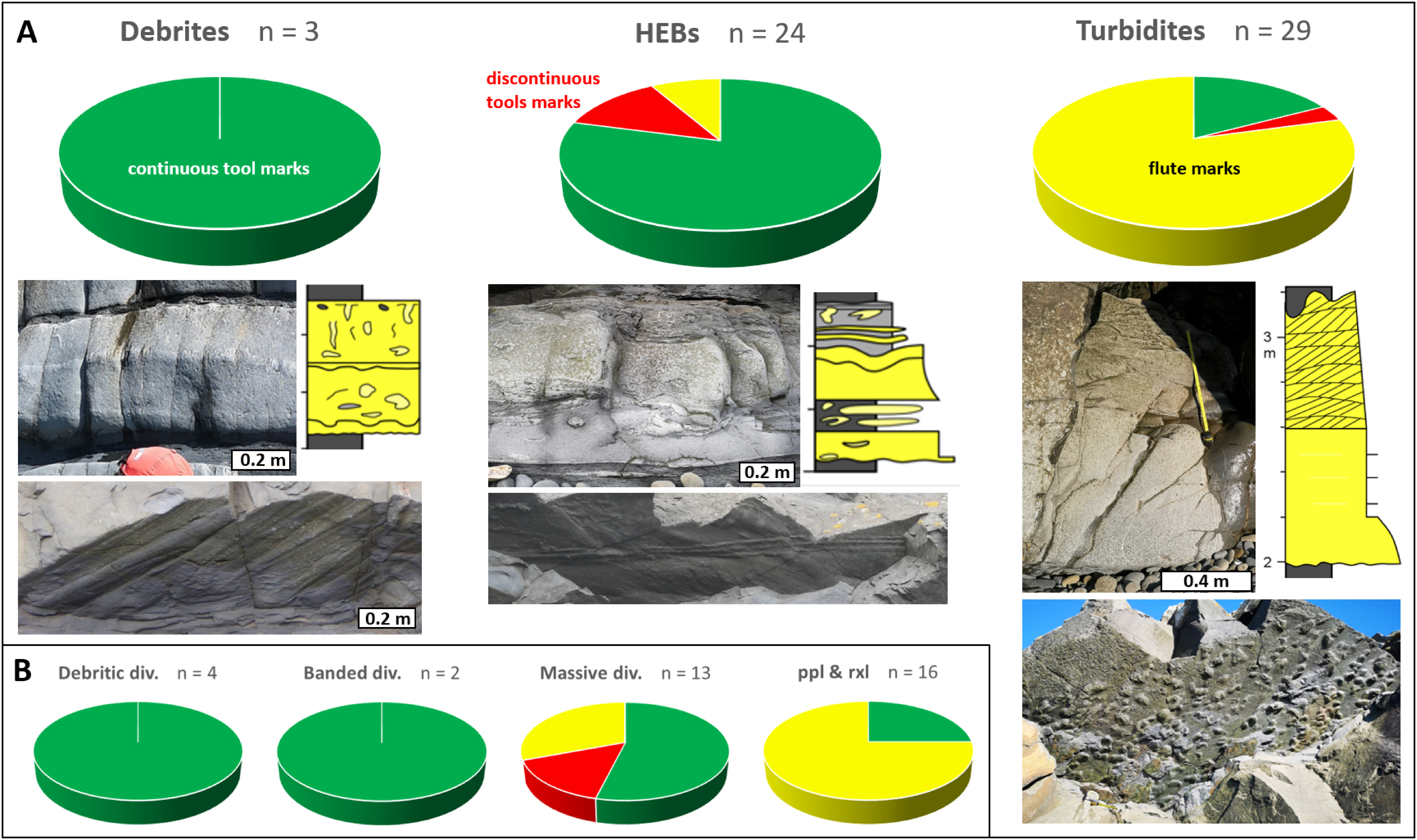
A
Debrites n = 3
HEBs n = 24
Turbidites n = 29
continuous tool marks
discontinuous
tools marks
flute marks
0.2 m
0.2 m
0.2 m
0.4 m
3
m
2
B
Debritic div. n = 4
Banded div. n = 2
Massive div. n = 13
ppl & rxl n = 16

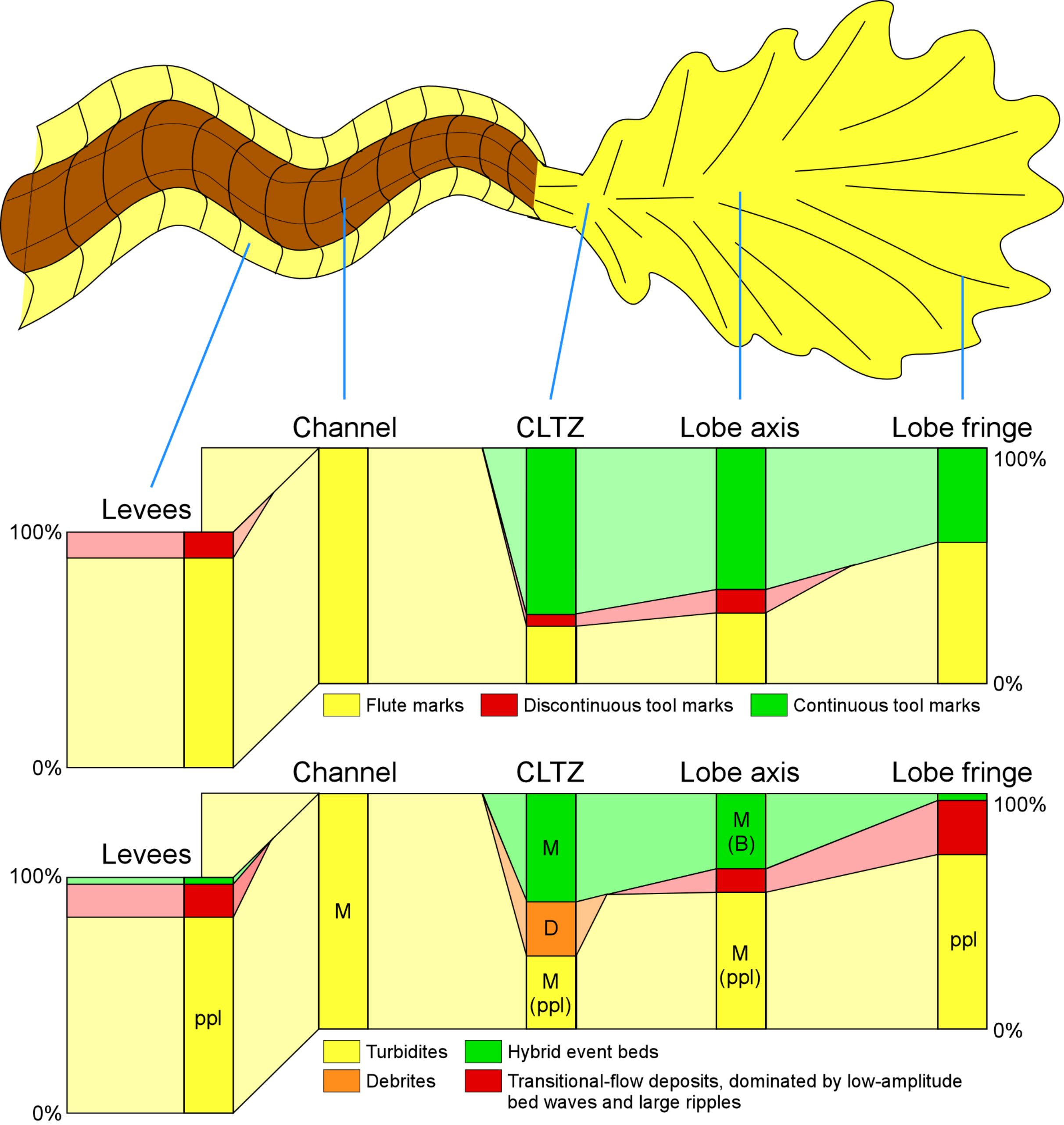

Channel
CLTZ
Lobe axis
Lobe fringe
Levees
100%
0%
100%
0%
Flute marks
Discontinuous tool marks
Continuous tool marks
Channel
CLTZ
Lobe axis
Lobe fringe
Levees
100%
0%
100%
0%
M
M
D
M
(ppl)
M
(B)
M
(ppl)
ppl
ppl
Turbidites
Hybrid event beds
Debrites
Transitional-flow deposits, dominated by low-amplitude
bed waves and large ripples

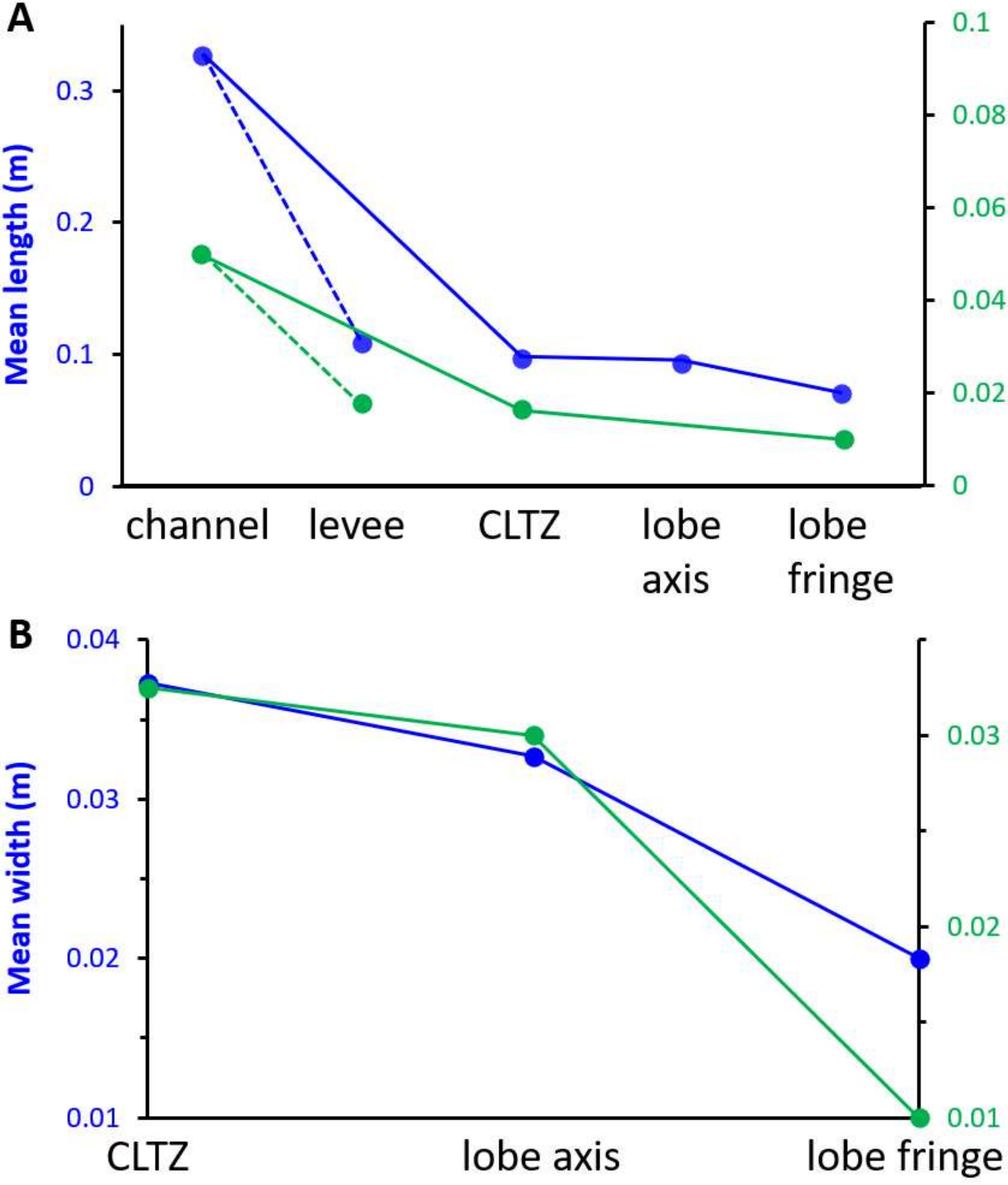

A
Mean length (m)
0.3
0.2
0.1
0
Mean depth (m)
0.1
0.08
0.06
0.04
0.02
0
channel
levee
CLTZ
lobe axis
lobe fringe
B
Mean width (m)
0.04
0.03
0.02
0.01
Mean depth (m)
0.03
0.02
0.01
CLTZ
lobe axis
lobe fringe

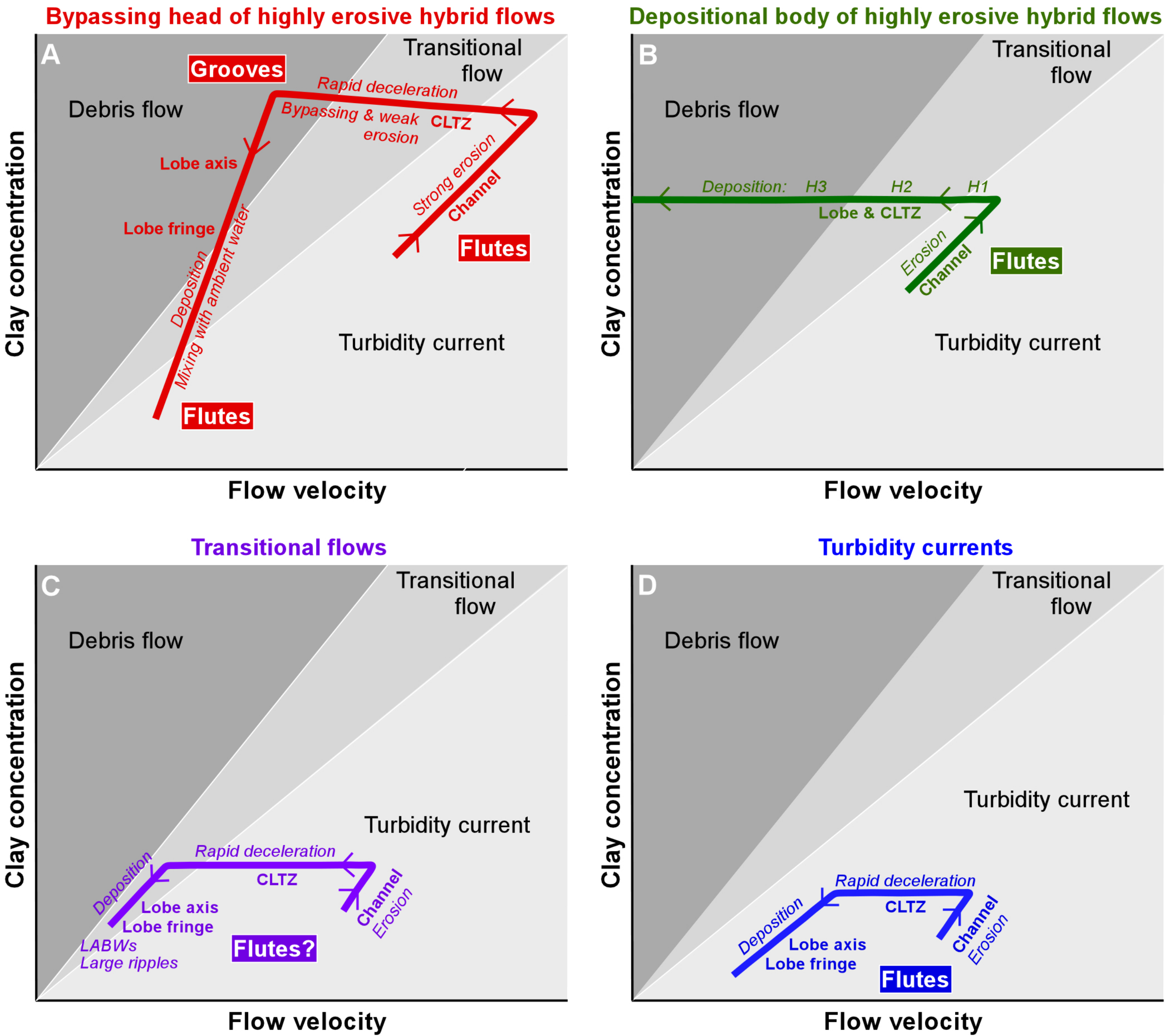
Bypassing head of highly erosive hybrid flows
A
Grooves
Transitional flow
Debris flow
Rapid deceleration
Bypassing & weak erosion
CLTZ
Lobe axis
Lobe fringe
Deposition
Mixing with ambient water
Strong erosion
Channel
Flutes
Turbidity current
Flutes
Clay concentration
Flow velocity
Depositional body of highly erosive hybrid flows
B
Transitional flow
Debris flow
Deposition: H3 H2 H1
Lobe & CLTZ
Erosion
Channel
Flutes
Turbidity current
Clay concentration
Flow velocity
Transitional flows
C
Transitional flow
Debris flow
Turbidity current
Rapid deceleration
Deposition
CLTZ
Lobe axis
Lobe fringe
Channel
Erosion
LABWs
Large ripples
Flutes?
Clay concentration
Flow velocity
Turbidity currents
D
Transitional flow
Debris flow
Turbidity current
Rapid deceleration
Deposition
CLTZ
Lobe axis
Lobe fringe
Channel
Erosion
Flutes
Clay concentration
Flow velocity

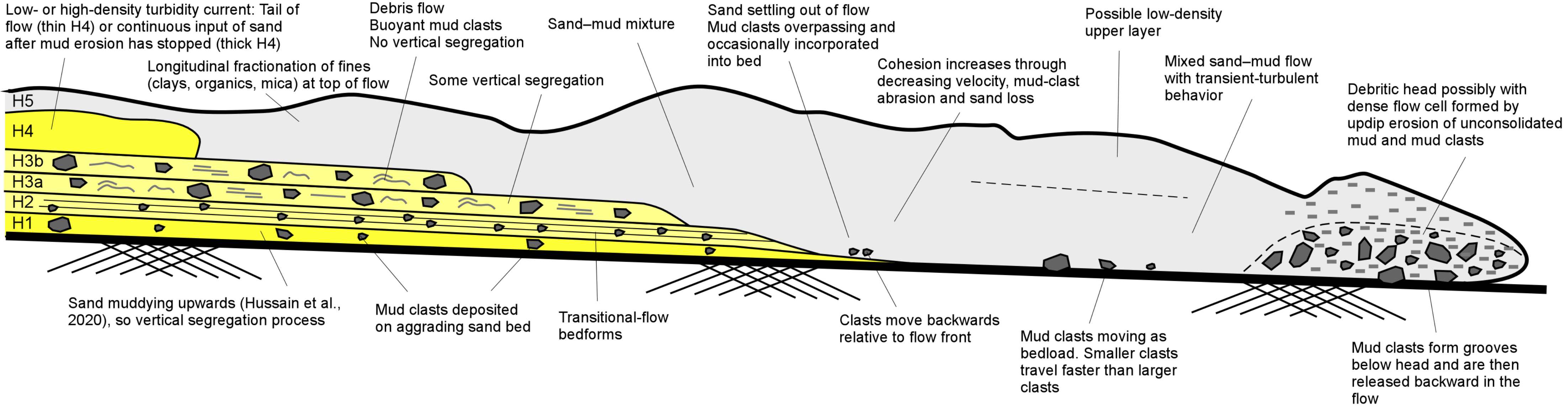

Low- or high-density turbidity current: Tail of flow (thin H4) or continuous input of sand after mud erosion has stopped (thick H4)
Debris flow
Buoyant mud clasts
No vertical segregation
Sand–mud mixture
Sand settling out of flow
Mud clasts overpassing and occasionally incorporated into bed
Possible low-density upper layer
Longitudinal fractionation of fines (clays, organics, mica) at top of flow
Some vertical segregation
Cohesion increases through decreasing velocity, mud-clast abrasion and sand loss
Mixed sand–mud flow with transient-turbulent behavior
Debritic head possibly with dense flow cell formed by updip erosion of unconsolidated mud and mud clasts
H5
H4
H3b
H3a
H2
H1
Sand muddying upwards (Hussain et al., 2020), so vertical segregation process
Mud clasts deposited on aggrading sand bed
Transitional-flow bedforms
Clasts move backwards relative to flow front
Mud clasts moving as bedload. Smaller clasts travel faster than larger clasts
Mud clasts form grooves below head and are then released backward in the flow

Table 1: Comparison of diagnostic properties of depositional environments in previous work and in the present study.

Depositional environment	**Diagnostic properties** (Spychala et al., 2017b, Brooks et al., 2018, Hansen et al., 2019)	**Diagnostic properties** This study	**Section**
Channel fill	• Base of channel-fill element is incised in underlying element • Medium to very thick, relatively coarse-grained event beds • Common amalgamation, very low mudstone content • Event beds have sharp, erosional or loaded base • Event beds fine in an upward direction • Sole marks and dewatering structures are common • Event beds thin in an upwards direction in the channel fill • Mostly deposits of high-density turbidity currents	• Base of channel-fill element is incised in underlying element • Thick-bedded and very-thick bedded sandstones and conglomerates, vertically graded from very coarse sand or granules to fine or very fine sand • Amalgamated event beds with erosional base, no mudstone • Large sole marks, dewatering structures, dune cross-bedding, load casts, and convolute bedding • Individual beds vary in thickness and pinch out laterally • Mostly deposits of high-density turbidity currents	4
Levee	• Thin-bedded sandstones and siltstones in hemipelagic mudstones • High proportion of climbing-ripple-laminated beds and ripple-cross-laminated beds (Kane and Hodgson, 2011) • Levee successions thin and fine upward • Mostly deposits of low-density turbidity currents	• Tabular, thin-bedded and very-fine grained or fine-grained sandstones • Cumulative mudstone bed thickness is 55% of total thickness • Sandstones are mud-poor, vertically graded, and rich in plane-parallel lamination, ripple cross-lamination, and convolute lamination • Mostly deposits of low-density turbidity currents	2
Channel–lobe transition zone	• Thin and discontinuous structureless and structured sandstones with climbing-ripple lamination • Lenticular, mostly thick-bedded, poorly sorted, clast- or matrix-supported sandstones and conglomerates with abundant intraformational mudstone clasts and rafts and sandstone clasts • Abundant soft-sediment deformation • Abundant scours, erosional surfaces (may be composite), and bypass lags	• Tabular, mainly thick-bedded sandstones and mixed sandstones–mudstones • Cumulative mudstone bed thickness is 20% of total thickness • Sandstones are fine- to medium-grained, with coarse- to very-coarse-grained basal divisions. Few beds are rich in granule-size clasts • Abundant convolute and contorted bedding, chaotic mixtures of sandstone and mudstone, mudstone rafts and clasts, sandstone clasts, vertical dewatering structures, load casts, and foundered sand • Plane-parallel lamination and ripple cross-lamination are confined to subordinate thin-bedded, fine- to very-fine grained sandstones and thin divisions in thicker sandstones • Some erosional contacts between amalgamated sandstones • Mostly hybrid event beds and transitional-flow deposits	1, 3, 7
Lobe axis and off-axis	• Massive thick-bedded amalgamated sandstones formed by high-density turbidity currents (lobe axis) • Medium-bedded turbiditic sandstones with plane-parallel lamination and (climbing) ripple cross-lamination (lobe off-axis) • Hybrid event beds (*sensu* Haughton et al., 2009) and quasi-laminar flow deposits (*sensu* Baas et al., 2011)	• Tabular, medium- and thick-bedded sandstones and mixed sandstones–mudstones • Cumulative mudstone bed thickness is 37% of total thickness • Maximum grain size in the sandstone ranges from fine sand to very coarse sand • Common convolute bedding, vertical dewatering structures, heterolithic sandstone–mudstone, chaotic mixtures of sandstone and mudstone, and plastically deformed sandstone • Few event beds with low-amplitude bed waves, crude banding, or mudstone clasts • Deposits of high-density turbidity current and hybrid event beds	6
Lobe fringe	• Thin- to medium-bedded, fine-grained turbiditic sandstones and siltstones • Lateral and frontal fringes are poor (< 2%) and rich (up to 33%) in hybrid event beds, respectively • Event beds are organized in lenticular sand-rich units, several meters thick	• Tabular, mainly thin- to medium-bedded and fine- to very fine-grained sandstones • Cumulative mudstone bed thickness is 44% of total thickness • Sandstones are vertically graded, with variable amounts of mud matrix • Common convolute bedding, low-amplitude bed-waves, and large ripples • Abundant deposits of low-density turbidity currents and few deposits of high-density turbidity current • Event beds tend to be organised in sand-rich units, several meters thick	5

Table 2: Overview of sole-mark data. Sole marks in bold refer to youngest type in beds with clearly crosscutting sole marks.

Depositional environment	Bed	Bed type	Lower division	Sole mark types
CLTZ	1a	turb hi	massive	skim
CLTZ	1b	debrite	debritic	**groove**; skim
CLTZ	1c	HEB sand	ppl	groove
CLTZ	1d	HEB mud	debritic	groove
CLTZ	1e	HEB	-	groove
CLTZ	1f	HEB	-	groove
CLTZ	1g	HEB	-	skim
CLTZ	1h	HEB	-	groove
CLTZ	1i	-	-	groove
CLTZ	1j	HEB	-	groove
CLTZ	1k	-	-	groove
CLTZ	1l	-	-	groove
CLTZ	1m	turb	-	flute(sp)
CLTZ	1n	-	-	groove
CLTZ	1o	turb	-	**flute(sp)**
CLTZ	1p	turb lo	ppl	flute(par,sp)
CLTZ	1q	-	-	**flute(par,sp)**; groove; skim
CLTZ	1r	HEB	-	flute(par); groove
CLTZ	1s	turb lo	ppl	flute(par,sp)
CLTZ	1t	turb	-	flute(sp)
CLTZ	1u	turb	-	flute(par)
CLTZ	1v	turb hi	massive	flute(par)
CLTZ	1w	turb	-	flute(sp); groove
CLTZ	1x	turb	-	flute(par)
Levee	2a	turb lo	ppl	flute(sp)
Levee	2b	turb lo	ppl	flute(par,sp)
Levee	2c	turb lo	ppl	flute(par,sp)
CLTZ	3c	HEB sand	massive	groove
CLTZ	3d	HEB sand	debritic	groove
Channel	4a	turb hi	massive	flute(par,sp)
Channel	4b	turb hi	massive	flute(par)
Channel	4c	turb hi	massive	flute(par)
Lobe fringe	5a	turb lo	ppl	**flute(par)**; groove; skip
Lobe fringe	5b	turb lo	ppl	**flute(par,sp)**; groove; skim
Lobe fringe	5c	turb lo	ppl	**flute(par)**; groove
Lobe fringe	5d	turb hi	massive	chevron; **groove**; skim
Lobe fringe	5e	turb lo	ppl	**groove**; skim; tumble
Lobe axis	6a	turb hi	massive	groove
Lobe axis	6b	HEB mud	massive	flute(par); groove; **skim**
Lobe axis	6c	HEB mud	banding	groove
Lobe axis	6d	HEB mud	massive	groove
Lobe axis	6e	turb lo	rxl	flute(par,sp)
Lobe axis	6f	HEB	-	groove
Lobe axis	6g	HEB	-	groove
Lobe axis	6h	turb	-	flute(par)
Lobe axis	6i	turb	-	flute(par)
Lobe axis	6j	HEB	-	groove
CLTZ	7a	HEB mud	massive	groove
CLTZ	7b	HEB sand	massive	groove
CLTZ	7c	turb hi	massive	groove
CLTZ	7d	HEB sand	banding	groove
CLTZ	7e	HEB sand	ppl	groove
CLTZ	7f	-	-	groove
CLTZ	7g	-	-	groove

Levee	2d	turb lo	ppl	flute(par)	CLTZ	7h	turb	-	groove
Levee	2e	HEB mud	ppl	flute(par,sp)	CLTZ	7i	-	-	groove
Levee	2f	turb lo	ppl	flute(asym,par)	CLTZ	7j	-	-	groove
Levee	2g	HEB	-	flute(par)	CLTZ	7k	HEB	-	groove
Levee	2h	HEB	-	flute(par); **skim**	CLTZ	7l	HEB	-	groove
Levee	2i	turb	-	flute(sp)	CLTZ	7m	-	-	flute(par)
CLTZ	3a	debrite	ppl	groove	CLTZ	7n	-	-	groove
CLTZ	3b	debrite	debritic	groove	CLTZ	7o	HEB	-	groove

turb = turbidite
lo = low density
hi = high density

HEB = hybrid event bed
mud = muddy H3 division
sand = sandy H3 division

ppl - plane-parallel lamination
rxl = ripple cross-lamination
par = parabolic

sp = spindle
asym = asymmetric
CLTZ = channel-lobe transition zone